SECOND QUARTERLY REPORT
VAPOR-CHAMBER FIN STUDIES

by

L. S. Langston
A. Sherman
B. H. Hilton

prepared for
National Aeronautics and Space Administration

Contract NAS3-7622

Pratt & Whitney Aircraft DIVISION OF UNITED AIRCRAFT CORPORATION

EAST HARTFORD • CONNECTICUT

NOTICE

This report was prepared as an account of Government sponsored work. Neither the United States, nor the National Aeronautics and Space Administration (NASA), nor any person acting on behalf of NASA:

A.) Makes any warranty or representation, expressed or implied, with respect to the accuracy, completeness, or usefulness of the information contained in this report, or that the use of any information, apparatus, method, or process disclosed in this report may not infringe privately owned rights; or

B.) Assumes any liabilities with respect to the use of or for damages resulting from the use of any information, apparatus, method or process disclosed in this report.

As used above, "person acting on behalf of NASA" includes any employee or contractor of NASA, or employee of such contractor, to the extent that such employee or contractor of NASA, or employee of such contractor prepares, disseminates, or provides access to, any information pursuant to his employment or contract with NASA, or his employment with such contractor.

Requests for copies of this report
should be referred to:

National Aeronautics and Space Administration
Scientific and Technical Information Facility
P.O. Box 33, College Park, Maryland 20740

NASA CR-54922
PWA-2773

SECOND QUARTERLY REPORT

VAPOR-CHAMBER FIN STUDIES

prepared for
National Aeronautics and Space Administration

January 1966

Contract NAS3-7622

Technical Management
NASA Lewis Research Center
Space Power System Division
Nuclear Power Technology Branch
Cleveland, Ohio
Martin Gutstein

Written by L. S. Langston — L. S. Langston, Asst. Proj. Engr.
A. Sherman — A. Sherman, Sen. Anal. Engr.
B. H. Hilton — B. H. Hilton, Anal. Engr.

Approved by H. R. Kunz — H. R. Kunz, Program Manager
W. J. Lueckel — W. J. Lueckel, Chief, Space Power Systems

Pratt & Whitney Aircraft DIVISION OF UNITED AIRCRAFT CORPORATION

EAST HARTFORD • CONNECTICUT

#36

FOREWORD

This report describes the work conducted from September 1, 1965 to November 30, 1965 by the Pratt & Whitney Aircraft Division of United Aircraft Corporation, East Hartford, Connecticut on Contract NAS3-7622, Exploratory Investigation of Vapor-Chamber Fin Concept for Space Radiators, for the Lewis Research Center of the National Aeronautics and Space Administration.

The work reported was conducted by H. R. Kunz, J. Barnes and the authors.

TABLE OF CONTENTS

TABLE OF CONTENTS (Cont'd)

LIST OF FIGURES

I. SUMMARY

This report describes the work completed during the second quarter of an experimental and theoretical program formulated for obtaining an understanding of vapor-chamber fins. During this period, wicking and boiling studies of porous materials applicable to fins were continued.

Twenty-three porous metal samples were selected for study and ordered from suppliers. Ten of these have been received and are now being tested in the wicking rise apparatus. In these tests, the liquid front in each sample is being observed by use of litmus paper strips spaced along the sample. The data obtained has shown that a relatively long time, in the order of days, is required for a liquid front in a sample to reach an equilibrium height.

The construction of the wick permeability apparatus was completed. Preliminary data has shown that K_1, the wick friction factor, was independent of time. This result indicates that dissolved gas was probably the cause of the time-dependent K_1 found by other investigators.

The apparatus for the wick boiling study was built and tested. Preliminary tests were run using a flat-plate sample. As yet no porous samples have been tested. A method of cutting these porous metal samples without disrupting the metal matrix has been devised.

II. INTRODUCTION

The purpose of the present study is to explore and define the mechanism of heat transport in the vapor-chamber fin. The program is divided into three basic parts, 1) wicking studies, 2) boiling studies, and 3) fin studies.

The work discussed in this second quarterly report deals with wicking and boiling studies. The purpose of the work is to evaluate the capillary and permeability characteristics of possible wicking materials for vapor-chamber fins, and to measure the boiling heat transfer characteristics of these materials. As discussed in the first quarterly report[1], the investigation of these phenomena will lead to a better understanding of the operation of the vapor-chamber fin.

The wicking materials that are under study are discussed in Section III, along with the methods of wicking material fabrication. The progress and the results of the capillary, permeability, and boiling tests are treated in Sections IV, V, and VI respectively. A discussion of future work is given in Section VII.

[1] First Quarterly Report, Vapor-Chamber Fin Studies, NASA CR-54882, PWA-2698, September 1965

III. WICKING MATERIALS

Four general classes of metallic wicking materials were considered for use as wicks in the fin. These are sintered screens, sintered powder, sintered fibrous structures, and flame-sprayed powdered coatings. During the reporting period, twenty-three wicks in these categories were selected for study, and samples were ordered from suppliers. These materials were selected on the basis of preliminary evaluation of capillary properties, permeability, ease of fabrication, dimensional stability, isotropy, chemical activity, and thermal conductivity. Four of the samples consist of sintered nickel screens, six of sintered nickel powder, and thirteen are constructed of either sintered nickel or sintered stainless steel fibers. No flame-sprayed powdered metal samples have been ordered or fabricated yet, since preliminary data on this porous material has shown that flame-sprayed metals have a wick friction factor that is much larger than those of the other types of porous media. This large friction factor is caused by an inherently low porosity. If further work validates these preliminary findings, no flame-sprayed samples will be studied. A description of each type of wicking material and a discussion of cutting methods for porous materials are included in Sections III. A. to III. D below.

A. Sintered Screen Samples

All four of the screen samples were received from the supplier and are now undergoing tests. Each of the four sintered screen samples consists of layers of nickel screen that have been pressed together against a nickel-foil backing and sintered together at points of contact in a furnace containing an ammonia atmosphere. The dimensions of each screen sample are shown in Figure 1. The following is a list of some of the properties of these screen samples.

TABLE 1

Properties of Sintered Nickel Screen Samples

Sample No.	Screen Mesh	Size, in.	Wire Dia., in.	Porosity, %
M7	50	18 x 2 x 0.10	0.009	62.5
M8	100	18 x 2 x 0.10	0.0045	67.9
M9	150	18 x 2 x 0.10	0.003	67.8
M10	200	18 x 2 x 0.10	0.0022	67.6

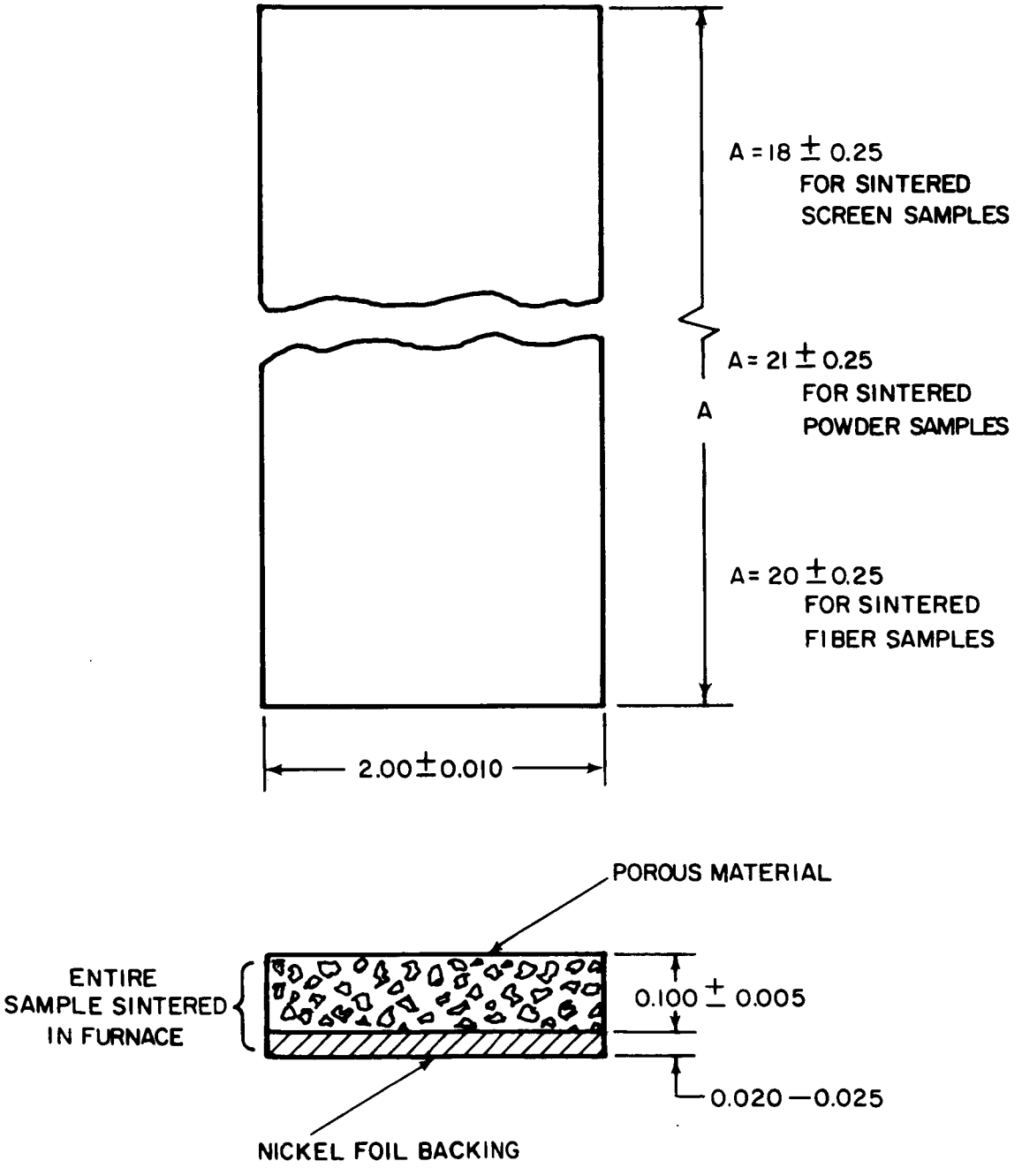

Figure 1 Dimensions of Porous Wicking Samples

The mesh referred to is the number of openings per linear inch in either the warp wire direction or the woof wire direction (since these are square-weave screen structures). The wire diameter is that of both the warp and woof wires.

The porosity is defined as the total void volume of the porous region of sample divided by the total volume of the porous region. Thus the porosities tabulated were calculated by using the equation:

$$\epsilon = \frac{V_T - \frac{W_T}{\rho_{Ni}}}{V_T} \qquad (1)$$

where

V_T = total volume of the porous region of the sample
W_T = total weight of the porous region of the sample
ρ_{Ni} = 8.90 gm/cc, the density of nickel

The weight and volume of the porous section of each sample were measured. A triple-beam balance, accurate to at least ±0.5 gm, was used to determine sample weight. Volume was determined by measuring the dimensions of the specimen with micrometers. Many measurements were taken of each dimension and a mean of these values was used to compute the volume. In all measurements and computations, the fact that the samples were backed by a solid nickel foil was taken into account. The uncertainty (i.e., confidence interval based on odds of 20 to 1) of the porosity values listed in Table 1 never exceeded ±1 per cent.

The porosities listed above yield some information about the way in which the screens are packed in each sample. In a layered screen structure there are two equilibrium positions that a square-weave screen could assume: a loose square stacking, and a close triangular stacking, shown in cross-section below.

Listed below each sketch is the calculated porosity that such a stacking would have if the warp and woof wires were bent as shown. If the porosities are compared with those in Table 1, the conclusion can be drawn that the actual screen stacking in the samples is quite close to the idealized square stacking model of the sketch above.

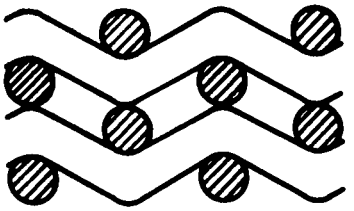

square stacking

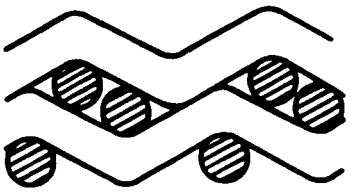

triangular stacking

Mesh	Wire Dia., In.	ϵ, %
50	0.009	61.2
100	0.0045	61.2
150	0.003	61.2
200	0.0022	62.3

Mesh	Wire Dia., In.	, %
50	0.009	43.6
100	0.0045	43.6
150	0.003	43.6
200	0.0022	45.0

Photomicrographs of the top view and cross-sectional view of sintered screen samples will be shown in the next quarterly report. Also, a pore size distribution curve will be determined for some samples, using a mercury intrusion porosimeter.

B. Sintered Powder Samples

Six wicking material samples constructed of sintered powdered nickel have been received from a supplier and are being tested. Figure 1 shows the dimensions of the sintered powder samples. These samples are made by compressing a powdered metal against a nickel foil backing using a die. The resulting sample is placed in a furnace with an ammonia atmosphere where the powder is sintered to itself and to the nickel foil backing. The nickel powder used to make each sample is termed an irregular powder, irregular in that the nickel particles in the powder were more needle-like than spherical. The length-to-diameter ratio of these needle-like particles is typically 4 or less.

In an irregular powder with its needle-like particles, the porosity can be varied over a fairly wide range from sample to sample. However, if a spherical powder is used, the porosity is restricted to fairly narrow limits. There are two forms in which spheres of equal diameter can be packed together stably, cubic and rhombohedric. The porosities of these packings are 47.84 and 25.95 per cent respectively. By using irregular powders rather than spherical regular powders, the porosity of sintered powdered samples can be greater than the 47.84 per cent that a spherical powder might impose.

The following is a list of some of the properties of the sintered powdered nickel samples.

TABLE 2

Properties of Sintered Powder Samples

Sample No.	Nominal Filter Rating, microns	Sieve Range, microns	Porosity, %
M1	20	150 - 297	59.7
M2	60	150 - 297	65.8
M3	100	297 - 841	47.7
M4	140	297 - 841	54.0
M5	180	297 - 841	69.1
M6	200	297 - 841	69.6

Metallic sintered powders are usually manufactured for a filtration use. Hence, instead of dealing with porosity and pore size distribution terms, filter manufacturers and users describe a porous material by a nominal filter rating. As an example of the use of this term, a 20-micron filter, when new, will ideally filter out of a flow 98 per cent of all 20-micron particles and all particles larger than 20 microns. It will pass 2 per cent of all 20-micron particles, and all particles smaller than 20 microns. To vary the nominal filter rating, a filter manufacturer can vary the powder size used for sintering and the density of packing (i.e., the porosity). To measure powder size he sifts it in a standard sieve. Thus the irregular nickel powder used in samples M1 and M2 will pass through a sieve with a square-weave screen whose openings are 297 microns across (a 50 Tyler standard sieve) but will not pass through a sieve with 150-micron openings (a 100 Tyler standard sieve). Similarly samples M3-M6 were sintered of irregular nickel powder that would pass through a screen with 841-micron openings (a 20 Tyler standard sieve) but not through a screen with 297-micron openings (a 50 Tyler standard sieve). Thus each wicking material sample listed above is composed of a range of powder sizes.

In lieu of a pore size distribution curve, a comparison of relative pore structure can be achieved from sample to sample by considering the nominal filter rating and the powder size range. For instance, it can be seen from Table 2 that samples M1 and M2 have a structure that is much finer than that of samples M3 to M6, although the former fall within the porosity range encompassed by M3 to M6.

The procedure followed in obtaining the porosity of each of the powdered nickel samples listed in Table 2 is the same as that described in Section III.A. Again, the uncertainty of the porosity values never exceeded ±1 per cent. The advantages of using an irregular powder for

samples M1 to M6 can be seen by the relatively high values of porosity that were obtained. In one powder size range (samples M3 to M6) the porosity varies from 47.3 to 69.8 per cent. The porosity is controlled by the density of packing. As with the screen samples, photomicrographs of the top view and cross-sectional view of sintered powder samples will be shown in the next quarterly report. Pore size distribution curves will also be measured for some of the more promising samples.

C. Sintered Fiber Samples

Thirteen sintered fiber samples have been ordered from a supplier. Like the screen and powder samples, these fiber samples are sintered to a metal foil backing. The dimensions of the fiber samples are shown in Figure 1.

The fiber samples are made from nickel or stainless steel which has been cut into fine fibers with length-to-diameter ratios in the range of 10 to 1000. These metallic fibers are felted to produce a randomly interlocked structure. The material is then sintered in a controlled-atmosphere furnace to produce metallic bonds at points where the fibers touch one another and the foil backing.

The fiber samples that have been ordered and some of their properties are tabulated in Table 3.

TABLE 3

Properties of Sintered Fiber Samples

Sample No.	Material	Mean Fiber Diameter, In.	Porosity, %	Mean Pore Diameter, microns
H1	nickel	0.0004	85	56
H2	nickel	0.0004	80	40
H3	nickel	0.0004	70	23
H4	nickel	0.0004	60	14
H5	nickel	0.0006	90	78
H6	nickel	0.0006	85	58
H7	nickel	0.0006	80	45
H8	nickel	0.0006	80	45
H9	nickel	0.0006	70	29
H10	nickel	0.0006	60	20
H11	430 stainless steel	0.0013	90	175
H12	430 stainless steel	0.0013	80	105
H13	430 stainless steel	0.0030	80	235

Since the fibers have a range of diameters in a given sample, a mean value of fiber diameter is listed in Table 3. Unlike the sintered screen and powder samples, porous materials formed of sintered metallic fibers can be made with extremely high porosities, as evidenced by the values listed in Table 3. Because of this property, sintered fiber metals appear very promising for use in the vapor-chamber fin.

The samples listed in Table 3 represent an overlapping range of both porosities and mean pore sizes. The mean pore sizes were obtained from the supplier who determined them by measuring the pore size distribution of each sample with a mercury porosimeter. Porosity and mean pore size are controlled by variation of the mean fiber diameter and the packing density of the fibers themselves.

When the fiber samples have been received from the supplier, testing will begin. As with other types of samples, photomicrographs of the top view and cross-sectional view of fiber samples will be shown in the next quarterly report. The porosity of all fiber samples will be measured and pore size distribution curves will also be measured for some of the more promising samples.

D. Cutting of Porous Materials

One of the problems encountered when dealing with porous metallic materials is that of cutting a sample without disturbing the porous structure in the region adjacent to the cutting plane. For the permeability and boiling tests of the present program many samples will have to be cut, since the samples used in these tests will be cut from the wicking samples shown in Figure 1, to insure the uniformity of wick samples from test to test. The edges of these samples must be open and undisturbed or the results of the tests will be greatly affected. A study was made of the various methods of cutting porous materials and it was found that there were very few methods available that do not disrupt the material structure near the region of the cut. Normal cutting techniques such as band-sawing, shearing, grinding and cutting with a torch usually smear the cut surface of a porous material, thereby sealing off pores in the material and decreasing its permeability. The most commonly used method to avoid this effect is that of filling the porous structure with a supporting material that can be removed following ordinary machining operations. The supporting material can range from a wax that is melted out after cutting, to a salt that is leached

from the structure in water. However, the filler material may not be completely removed or the filler can change the wetting characteristics of the porous material.

Electro-discharge machining (EDM) was therefore considered. EDM is a process of metal removal brought about by causing an electrical spark to jump a gap between the work piece and an electrode. A dielectric material flows between the electrode and the work piece, both to cool the work and to remove the spark-eroded particles as they come off the work piece. This technique was tried and found to produce a rather rough, irregular, cut edge.

The most promising cutting method and the one which is being considered for use at present is that of electrochemically machining a porous material. Electrochemical machining (ECM) is essentially metal removal by controlled electroplating in reverse. The work piece and a shaped tool form a pair of electrodes. An electrolyte (usually an ordinary salt solution) is pumped between the work piece and the tool and a voltage is applied to them. The material of the work piece is then removed by electrolysis, duplicating the shape of the tool. The electrolyte sweeps away the metal ions so that they cannot deposit out on the tool, which acts like an anode. This cutting process occurs at the temperature of the electrolyte so there is no excessive temperature at the cut surface. Also, because of the electrolysis process all chemical reactions take place right at or near the surface being produced, rather than in the matrix of the porous material.

When examined under a microscope, porous metal surfaces produced by electrochemical machining exhibit a minimum of disruption. Also, preliminary permeability tests indicate that there are no frictional end effects with an ECM-cut sample. At present, tooling for the electrochemical cutting of boiling and permeability samples is being designed and built.

IV. WICKING RISE TESTS

In the first quarterly report it was shown that the wicking rise tests provide a measurement of the maximum pumping force that a wicking material can produce. This is determined by measuring the maximum height to which a liquid will rise in a given vertical wicking material sample. During the second quarter the wicking rig described in first quarterly report was modified and some of the samples listed in Section III were tested. This section contains a discussion of these modifications and the results obtained.

A. Wick Liquid Front

Due to the surface finish and the opacity of the materials tested, it was found that it was not possible to visually observe the liquid front in a given wick. As related in the last quarterly report, various methods of measuring the position of the liquid front were tried, the best one being that of attaching litmus paper to the wick and noting when the paper was first wet.

The litmus paper method has since been refined by adding a small amount of potassium hydroxide to the water to increase the response of the litmus paper. Tests were made to find the smallest amount of basic material that could be added to the water and still cause pink litmus paper attached to a wick to turn to a vivid blue. It was found that a solution 0.03 per cent by weight of KOH was adequate for this result. This wicking liquid can be treated as being essentially pure water, due to the very small amount of KOH used. Figures 2 and 3 show that the interfacial properties of aqueous solution of 0.03 per cent of KOH differ insignificantly from those of pure water.

The litmus paper in the form of thin strips is held against the surface of the porous sample by a Plexiglas ladder. The ladder and the sample are held together by rubber bands which are placed around the assembly at various points. A picture of a wick sample both with and without the ladder is shown in Figure 4. The Plexiglas ladder shown in the sketch below, is made by machining rectangular grooves into a 1/8-inch thick

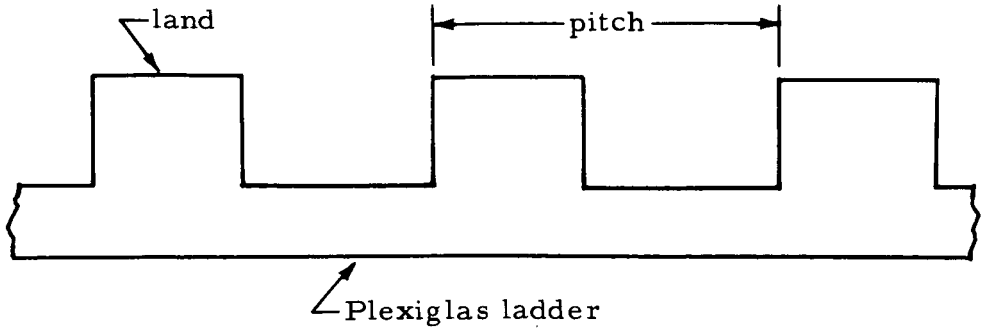

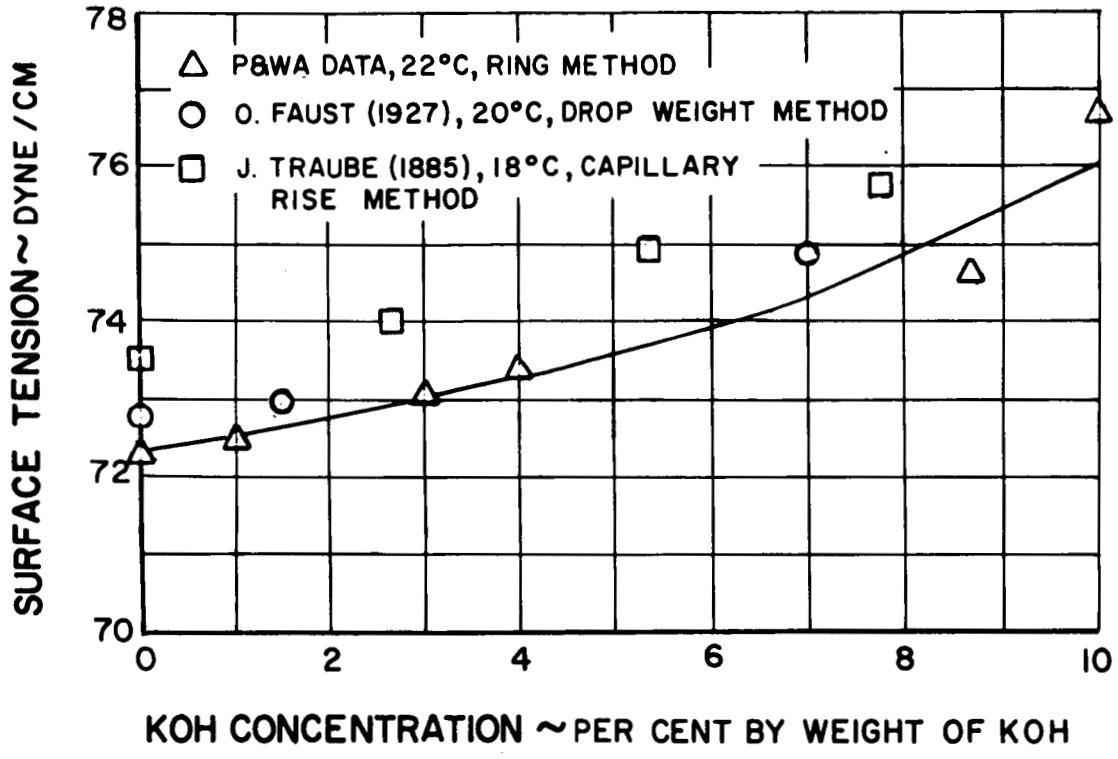

Figure 2 Surface Tension of Aqueous KOH Solutions vs KOH Concentration

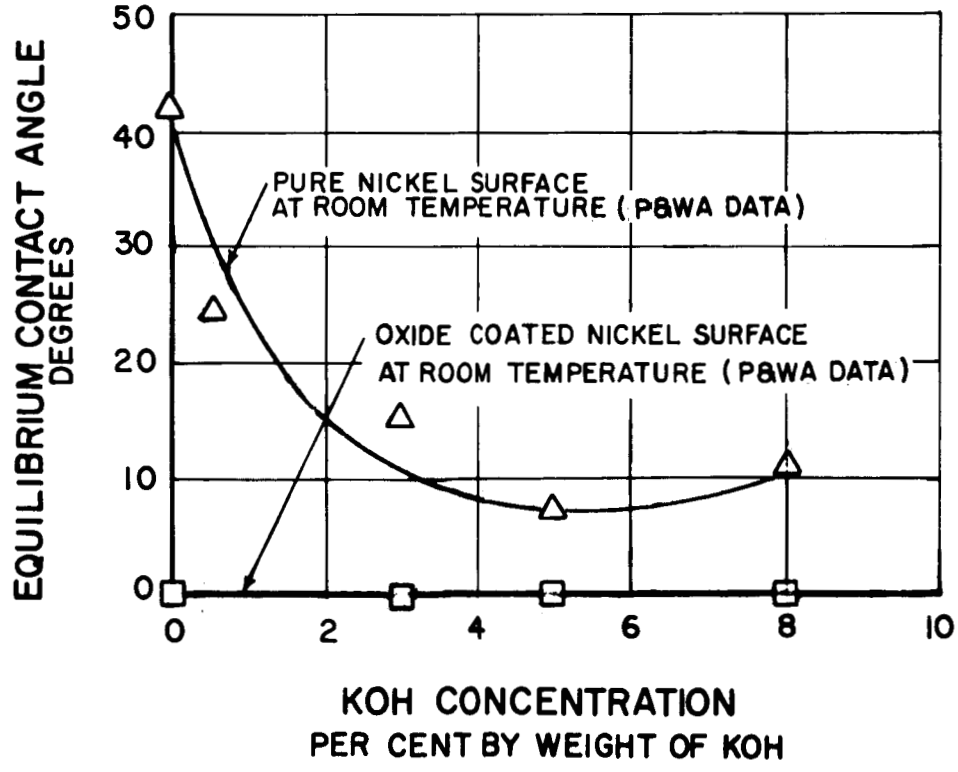

Figure 3 Equilibrium Contact Angle of Aqueous KOH Concentration for Two Nickel Surfaces

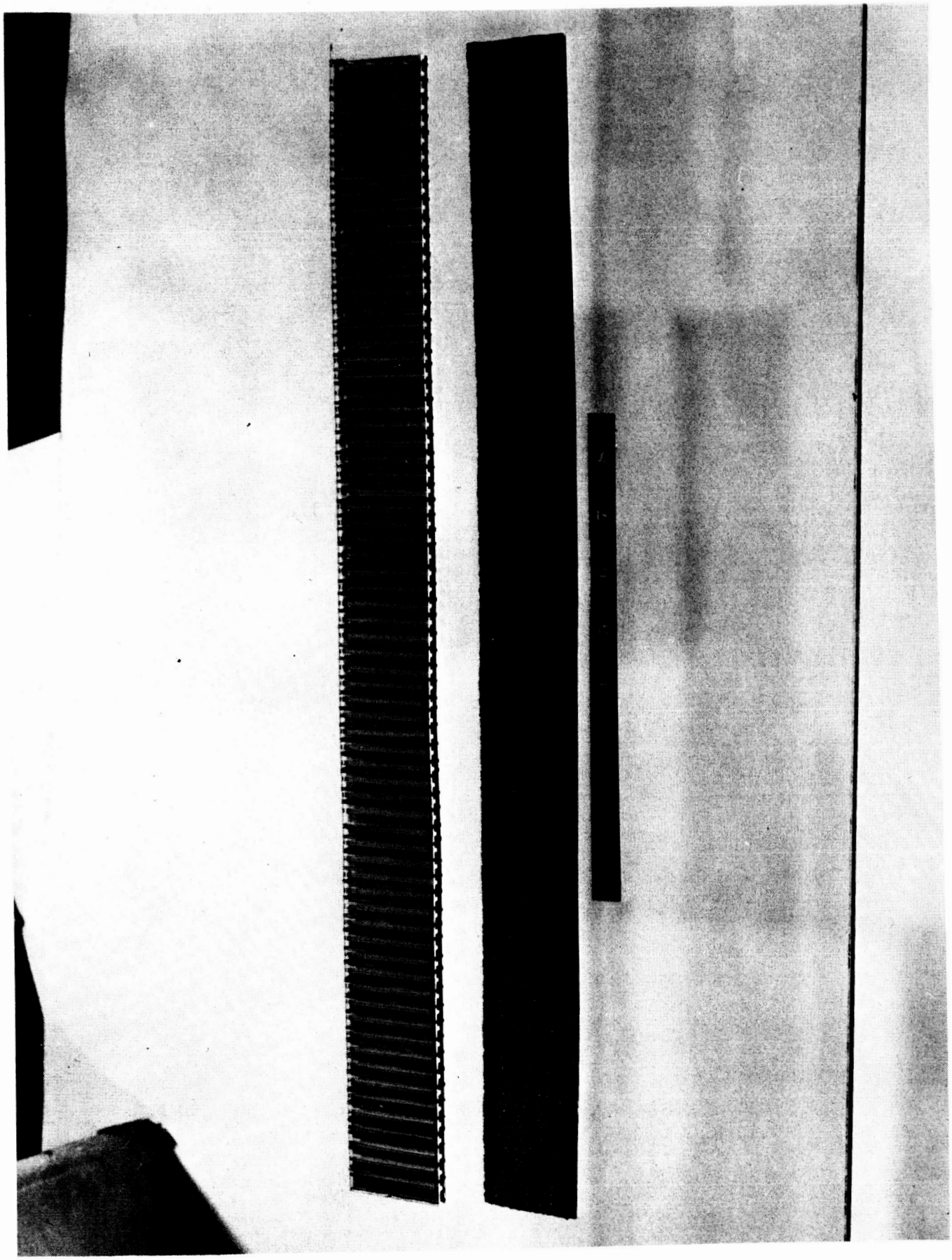

Figure 4 Wicking Samples with and without Litmus Paper

sheet of acrylic plastic, resulting in lands about 0.08-inch wide for holding the strips of litmus paper. The first ladders had a land pitch of 0.5 inch, but later the pitch was set at 0.3 inch. On a sample 20 inches long there are 66 strips of litmus paper approximately 0.1 inch wide, one under each land. The grooves in each Plexiglas ladder are 0.08 inch deep, making the ladder very flexible. When rubber bands are wrapped around it and the sample, the ladder conforms to the local irregularities of the porous sample, thereby pressing the litmus strips against the sample surface for good contact.

There are two drawbacks to the use of the litmus paper. One is that the litmus paper does not respond instantaneously to the position of the actual liquid front when the front first reaches the level of a given strip. It takes a finite amount of time to wet the paper and to react with the pH indicators in the litmus paper. The measured rate of rise curve is then lower than the rate of rise curve of the actual liquid front in the sample. However, for elapsed times of an hour or longer, this difference is negligible, as will be shown.

The other drawback is the fact that each strip is separated by a finite distance of 0.30 inch. Thus the finest division for measuring the height of the liquid front is this spacing. It was felt that any closer spacing would introduce too much litmus paper, which in itself is an excellent wick and might influence test results. However, with moderate wicking heights of 6 inches, this error of +0.30 inch -0.00 inch amounts to an uncertainty of only +5 per cent -0 per cent in measured values of maximum wicking rise, l_m.

B. Wicking Rise Apparatus and Test Procedure

The wicking rise apparatus is shown in Figure 5. It is the same as described in the first quarterly report except that a Plexiglas reservoir replaces the glass reservoir. The Plexiglas reservoir is completely covered and has rubber sleeves through which the glass tubes fit. In this way the contamination and evaporation of the liquid are kept to a minimum.

The results of the wicking tests have shown that it can take a long time, i.e., days, for the liquid front in a wicking sample to reach an equilibrium height. Some of the denser porous metal samples did not reach an equilibrium height in 20 days. Similar results have been

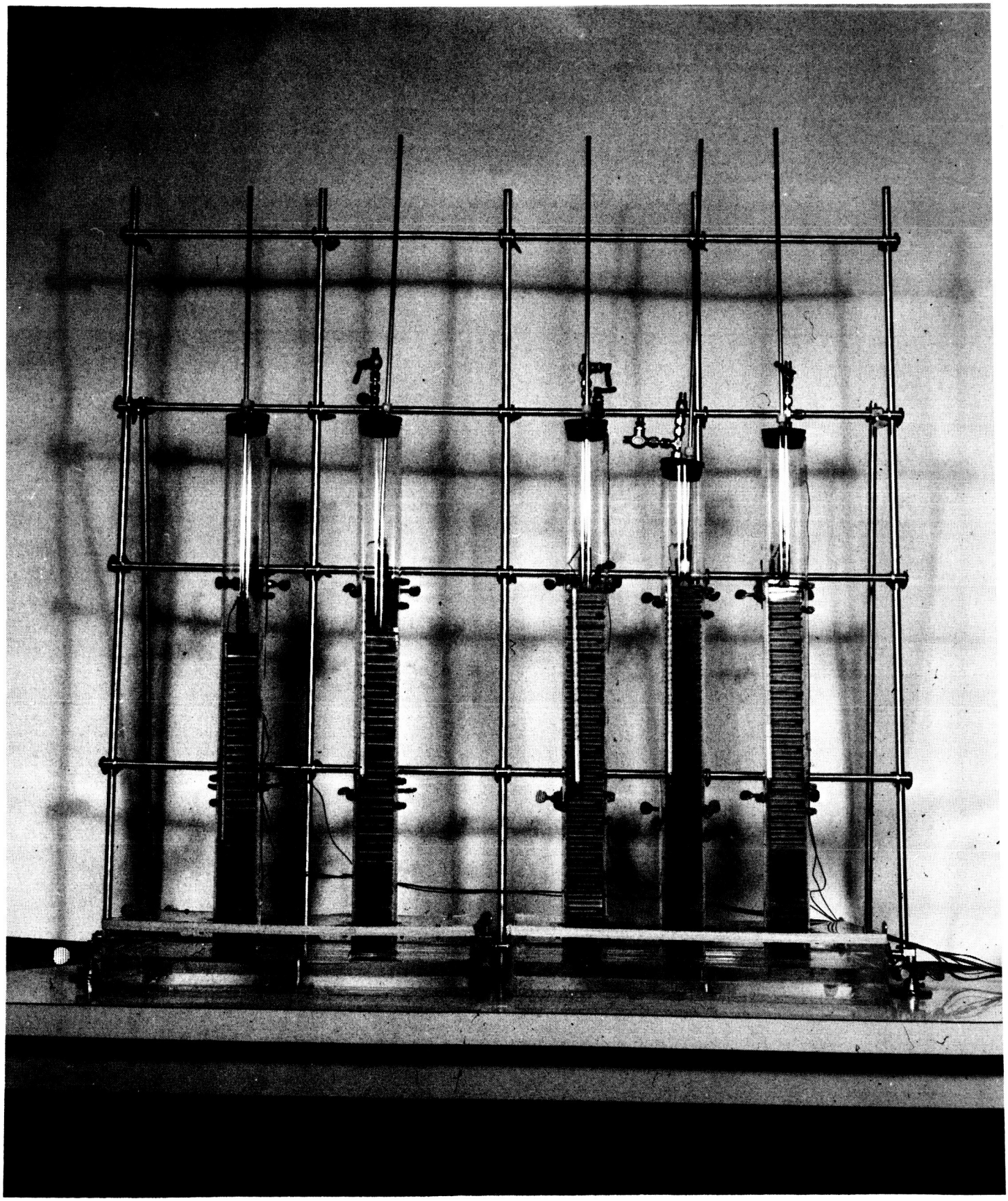

Figure 5 Wicking Apparatus with Samples Installed

obtained by other investigators[1]. Generally, after the first few hours of a wicking test, the rate of rise of the liquid front becomes very small and increasingly difficult to see. Because of the small amount of liquid present at the higher levels in the sample, it is quite important to enclose the wick in a saturated-vapor environment to prevent mass transfer. Failure to eliminate the latter would cause a low value of l_m, the equilibrium height, to be recorded.

Another modification to the apparatus is shown in Figure 6. This consists of a large triple-layered cardboard enclosure that fits over the entire apparatus. As shown, the box has a Plexiglas window, through which the samples may be viewed. The purpose of the enclosure is to maintain the apparatus at a near constant temperature and to minimize any temperature gradients along each tube.

During earlier tests it was found that the temperature gradient along each tube could amount to as much as 4°F. This not only caused errors in estimating surface tension but also caused condensation to form on the inside of each tube, making the reading of the liquid level in each sample difficult. To remedy this, thermocouples were attached to the outside of three of the tubes, at the top, middle, and bottom. Thermocouples were also placed in each of the two liquid reservoirs. After the enclosure described above was installed, the temperature gradient along each tube decreased to less than 1°F, and condensate no longer formed in the tubes.

Figure 7 shows three samples during a test. The following test procedure is used.

> At time zero, the end of each wick is lowered into the aqueous KOH solution. The time and temperatures are recorded every time a litmus strip turns blue (indicating contact with the 0.03 per cent KOH solution liquid front). After the liquid rise rate decreases to less than 0.3 inch/hr, readings are taken every hour. The test continues until the rate of liquid rise has become less than 0.1 inch per day, the liquid front reaches the top of

[1] Ginwala, K., T. A. Blatt, and R.W. Bilger, Engineering Study of Vapor-Cycle Cooling Components for Space Vehicles, Tech. Doc. Rept. No. ASD-TDR-63-582, Sept. 1963, AF Flight Dynamics Laboratory, Air Force Systems Command, Wright-Patterson Air Force Base, Ohio, pp 120-148

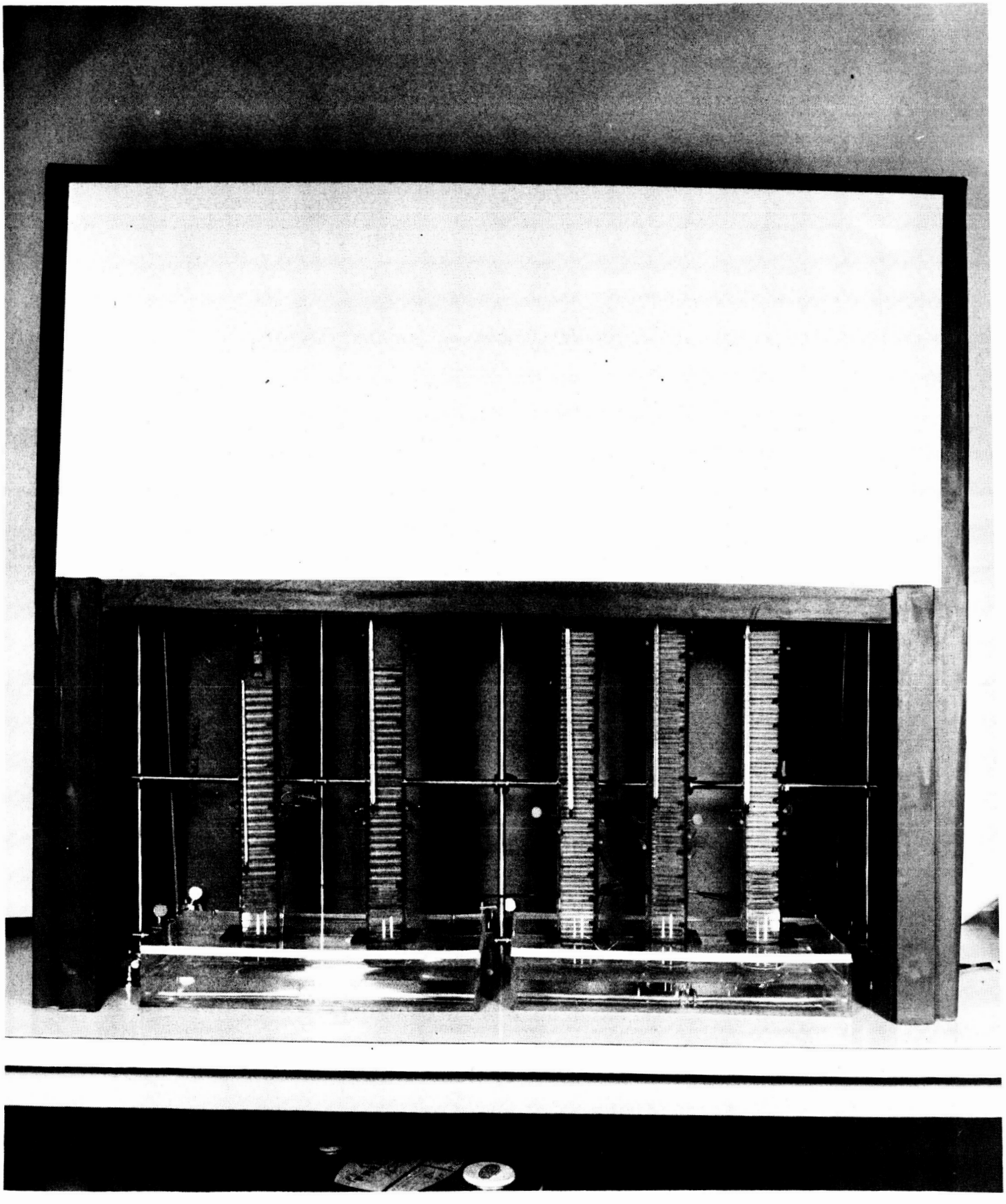

Figure 6 Wicking Apparatus in Insulating Enclosure

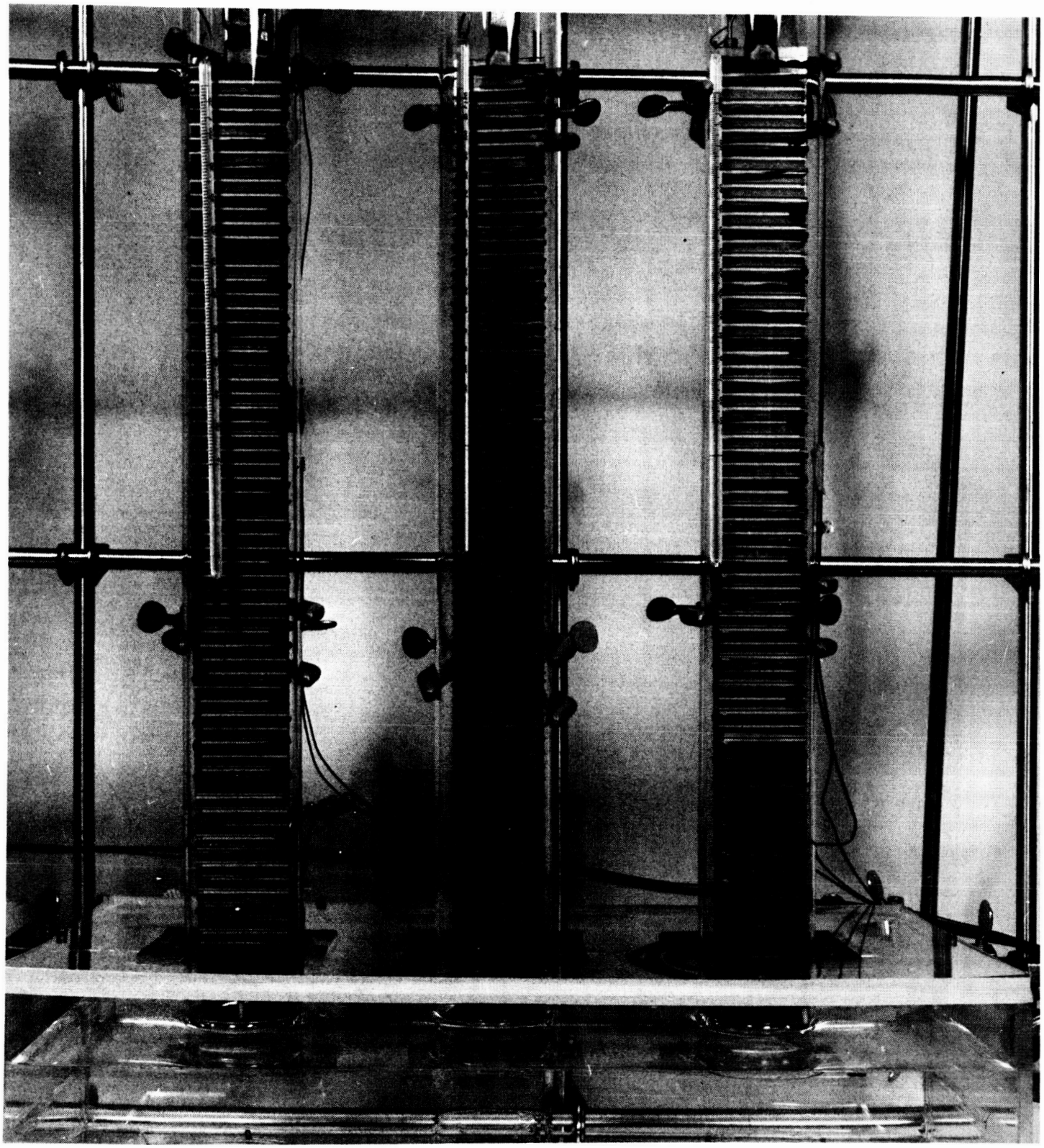

Figure 7 Closeup of Three Wicking Samples during Test

the sample, or a period of two weeks elapses. Each sample is subjected to a cleaning procedure before being tested in the maximum wick rise apparatus. This procedure consists of

1) washing the sample in a vapor degreaser and immediately rinsing in distilled water,
2) bathing the sample in a reagent-grade acetone bath,
3) rinsing the sample several times in distilled water, and
4) drying the samples for about two hours in an oven at 500°F.

C. Test Results

At present, samples M1 through M10 have been or are in the process of being tested. Samples H1 through H13 have not been received from the supplier yet. To insure accurate results, each sample will be tested at least twice. However, due to the length of time required for a wicking test, two tests have not been accomplished yet for any sample.

Test data for samples M8, M2, and M1 are shown in Figures 8 to 10. Figure 8 is a rate of rise curve for sample M8, the 100-mesh screen. Due to the long times necessary to reach equilibrium, a semilog plot is required to determine whether a true equilibrium height has been reached. The usual linear plot is misleading in that an apparent asymptote is reached before a true equilibrium height has been attained. Figure 9 shows rate of rise data for sample M2, a 60-micron sintered powder sample. Due to its smaller pore size, the liquid front rises higher and at a slower rate than that shown in Figure 8. The rate of rise data for a still denser sample with smaller pore size is shown in Figure 10. As indicated by the data shown, the liquid front in this sample (sample M1) did not reach an equilibrium height in 20 days.

In all of these plots each data point shown represents the time at which the strip of litmus paper was observed to change color. The last data point represents the level read when the particular test was terminated. In each plot the departure from the curve of the data points for times less than one minute is due to the lag between the time of the actual passage of the liquid front and the observed change in the color of the litmus paper.

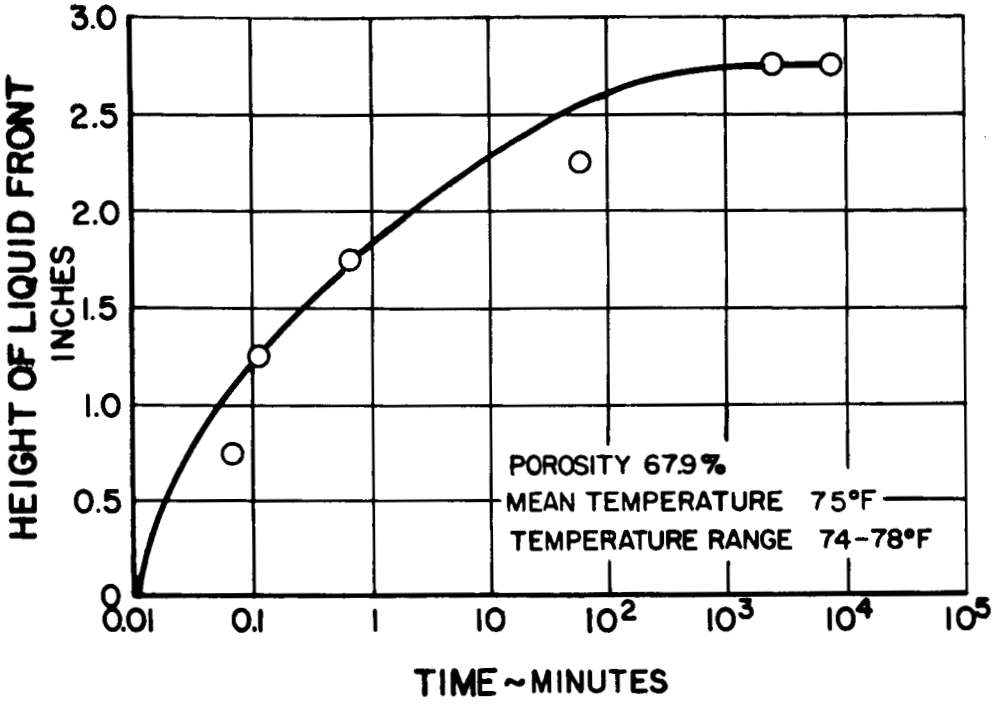

Figure 8 Wicking Curve for 100-Mesh Sintered Nickel Screen Sample M8

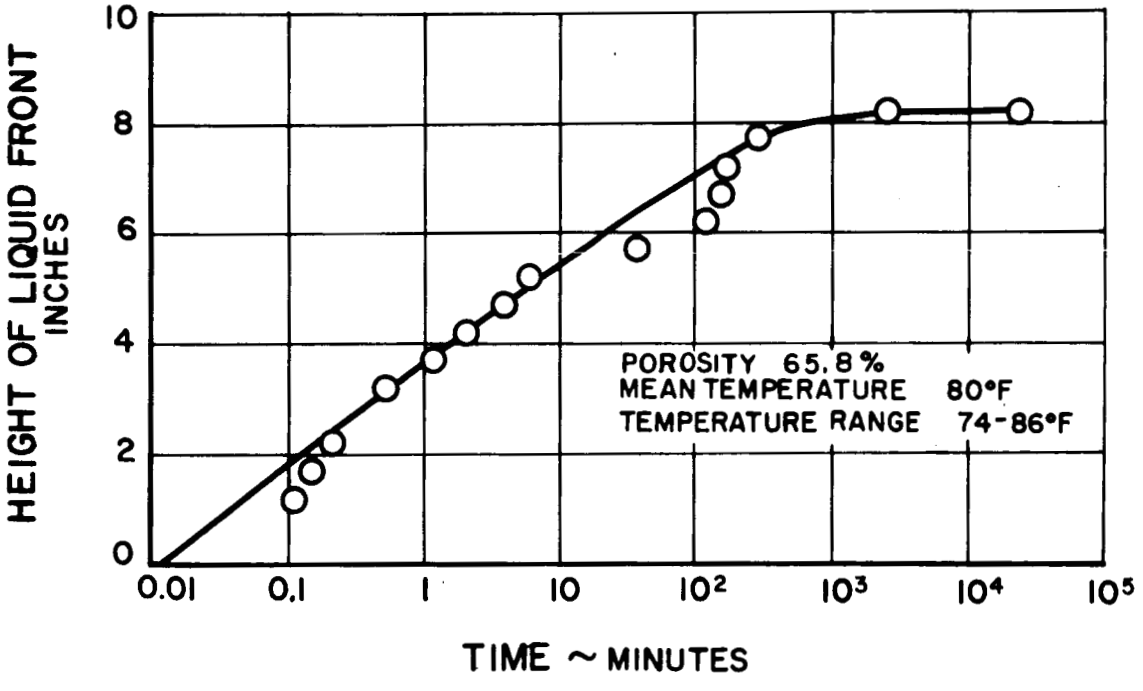

Figure 9 Wicking Curve for 60-Micron Sintered Nickel Powder Sample M2

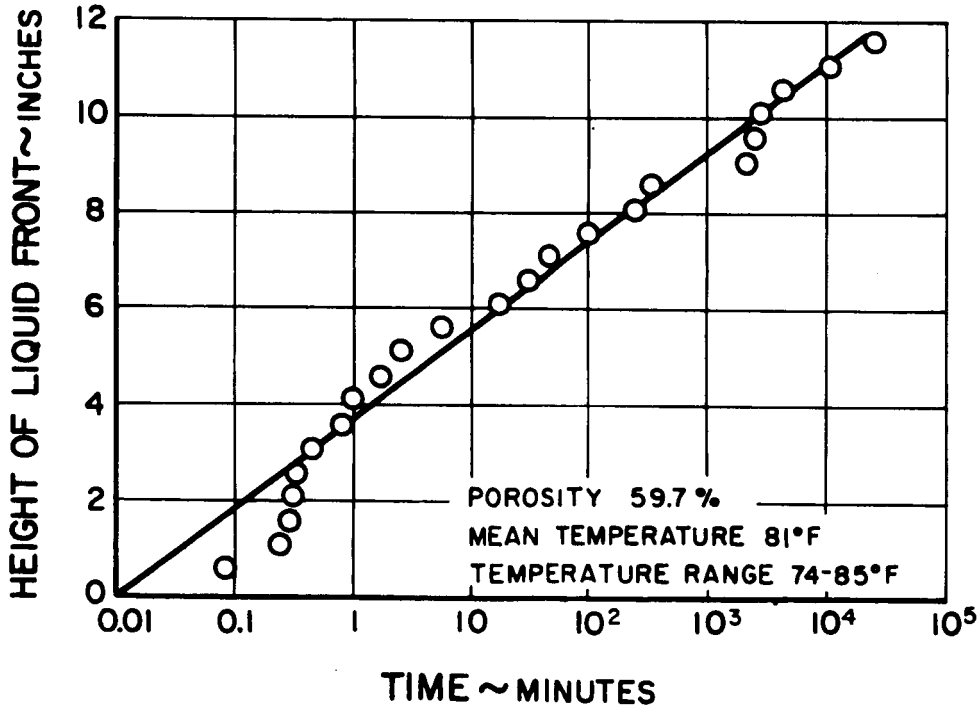

Figure 10 Wicking Curve for 20-Micron Sintered Nickel Powder Sample M1

V. WICK PERMEABILITY TESTS

The permeability apparatus is designed to evaluate the friction factor K_1 for liquid flow through wicks. Either water or Freon 113 flows through a wick specimen of known size and the flow rate, pressure drop and temperature of the liquid measured. These values are used to calculate K_1 from the equation given in the first quarterly report:

$$K_1 = \frac{A_c \rho_L \Delta P}{\Delta x \mu_L w_L}$$

where A_c is the cross-section area of the wick normal to the flow, Δx is the flow length of the wick, ρ_L and μ_L are the density and viscosity respectively of the liquid, ΔP is the pressure drop of the liquid across Δx, and w_L is the flow rate of the liquid through the wick. The objective of the permeability tests is to evaluate K_1 as a function of the type of wick flow rate, temperature, and time.

If Darcy's law for the flow of a fluid in a porous medium holds, K_1 will be determined by the geometry of the wick only, and will be independent of flow rate, temperature, and time, as well as the fluid used. This section describes the apparatus and the procedure used to determine K_1 and the results obtained to date.

A. Description of Permeability Apparatus

1. Permeability Samples:

Permeability samples are cut from the wicking samples shown in Figure 1. The overall dimensions of each sample are 0.100-inch thick by 2.0 inches wide, with a flow length of 3.0 inches. Each sample is supported on a backup plate 0.025 inch thick, 2.0 inches wide, and 3.0 inches long. Figure 11 shows a permeability sample with the sample holder disassembled.

2. Test Assembly:

A schematic of the permeability apparatus in its present form is shown in Figure 12. The apparatus consists of a closed-loop fluid system with a mechanical pump forcing a liquid through a wick. The wick is enclosed by gaskets in a sample holder so that flow occurs through the wick parallel to the 3.0-inch wick dimension. Variable-area flowmeters are used to measure flow

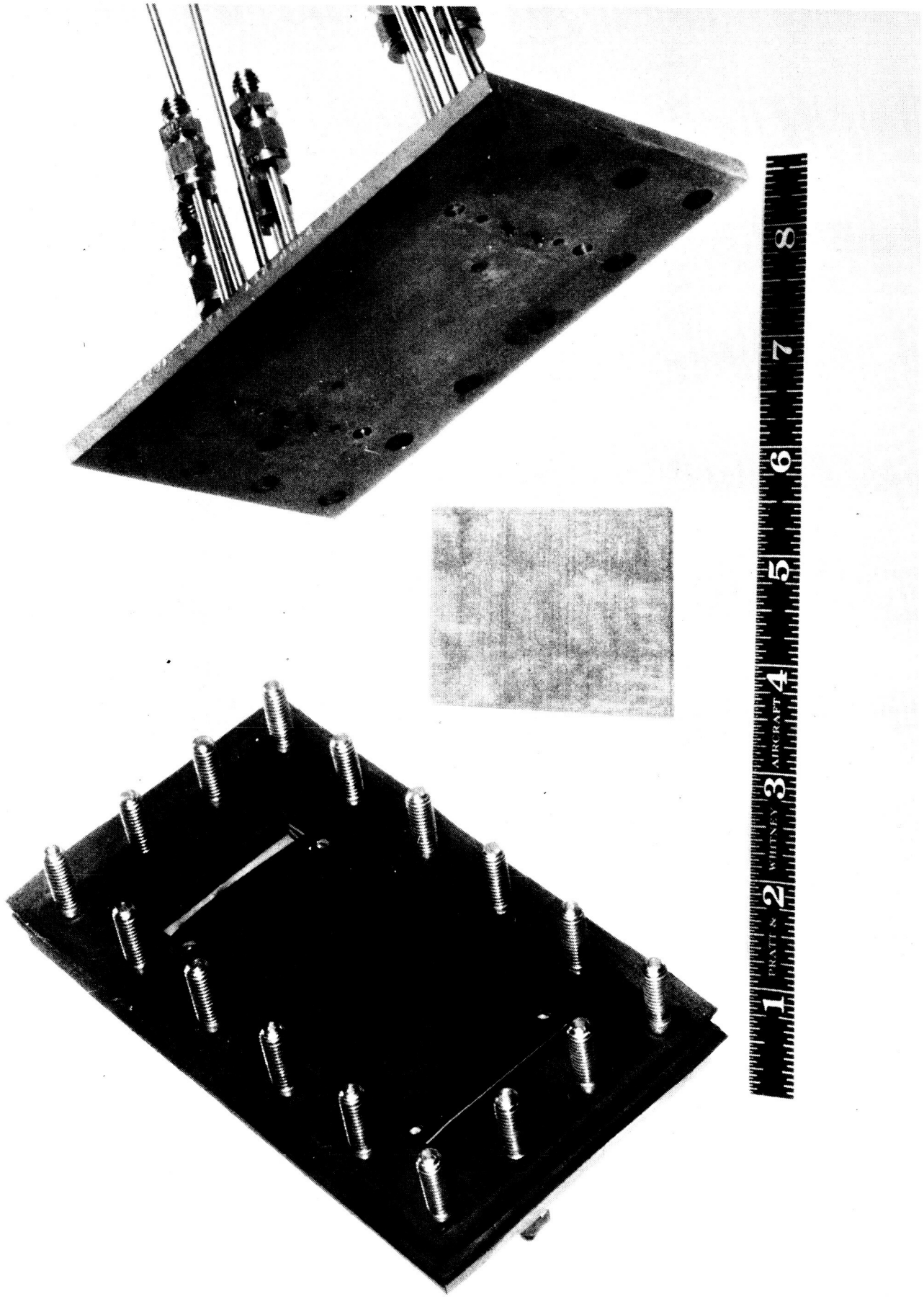

Figure 11 Disassembled Sample Holder with 150-Mesh Sintered Screen Permeability Sample

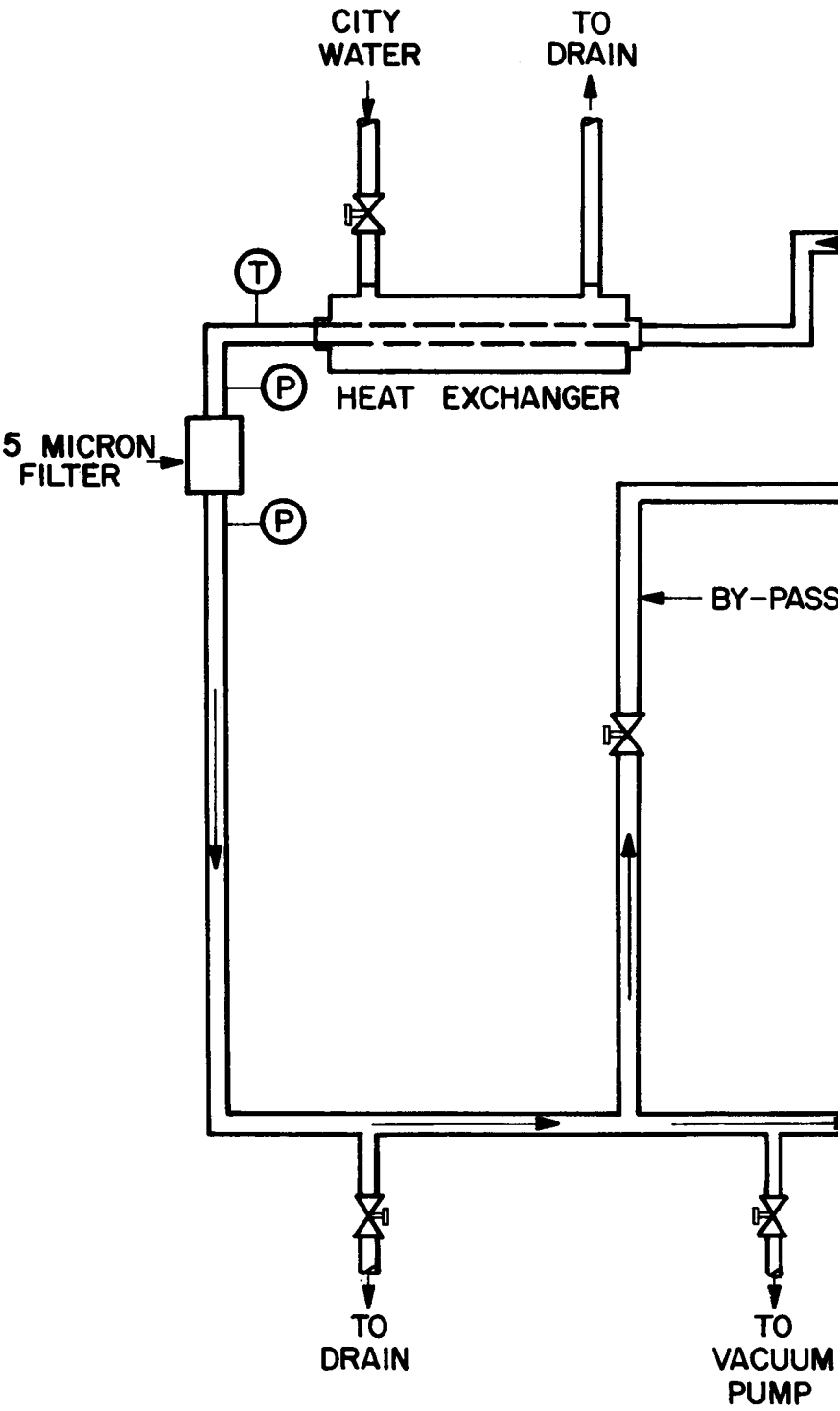

Figure 12 Schematic Diagram of Permeability App

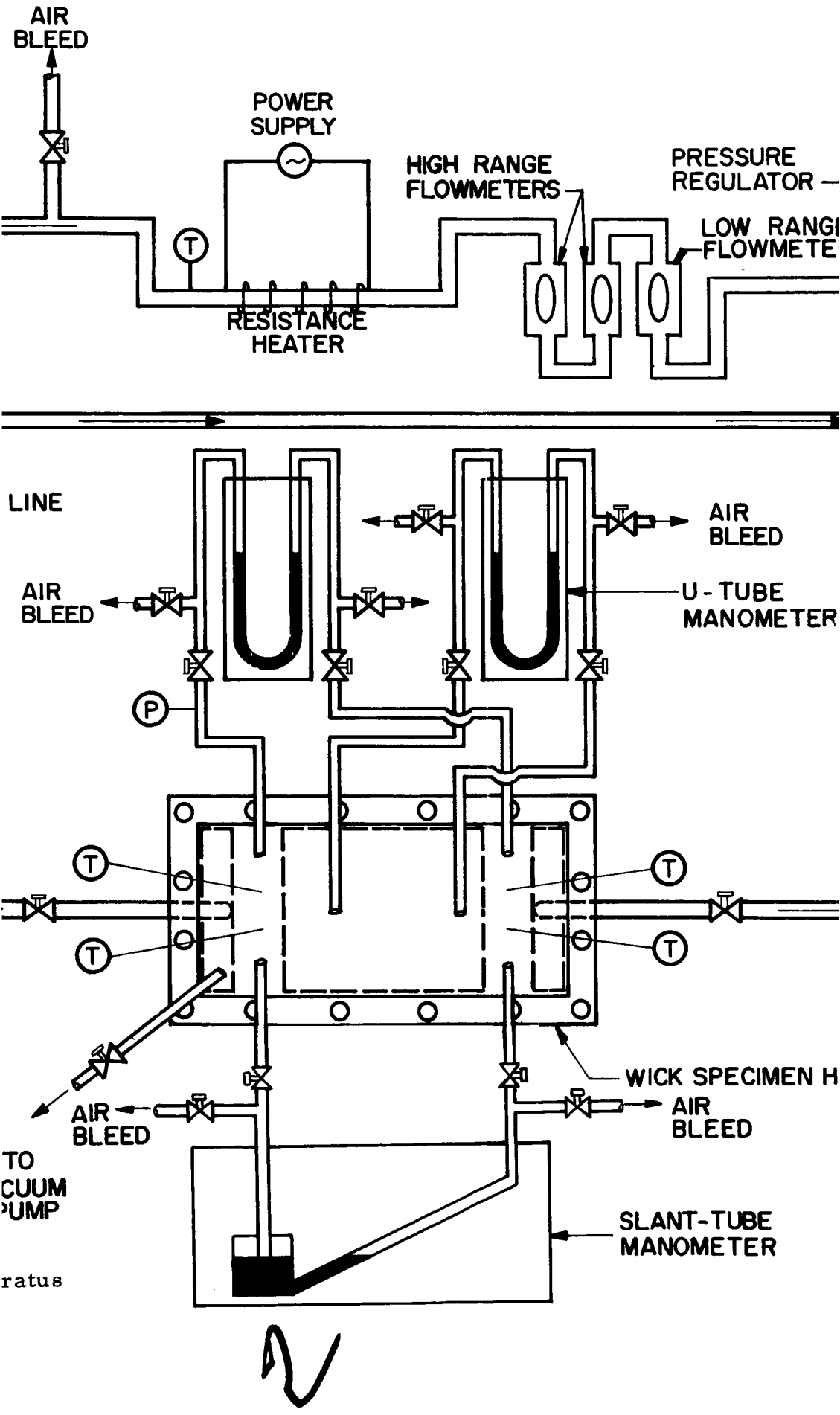
AIR
BLEED
POWER
SUPPLY
HIGH RANGE
FLOWMETERS
PRESSURE
REGULATOR
LOW RANGE
FLOWMETER
T
RESISTANCE
HEATER
LINE
AIR
BLEED
AIR
BLEED
U-TUBE
MANOMETER
P
T
T
T
T
WICK SPECIMEN H
AIR
BLEED
AIR
BLEED
TO
CUUM
UMP
SLANT-TUBE
MANOMETER

ratus

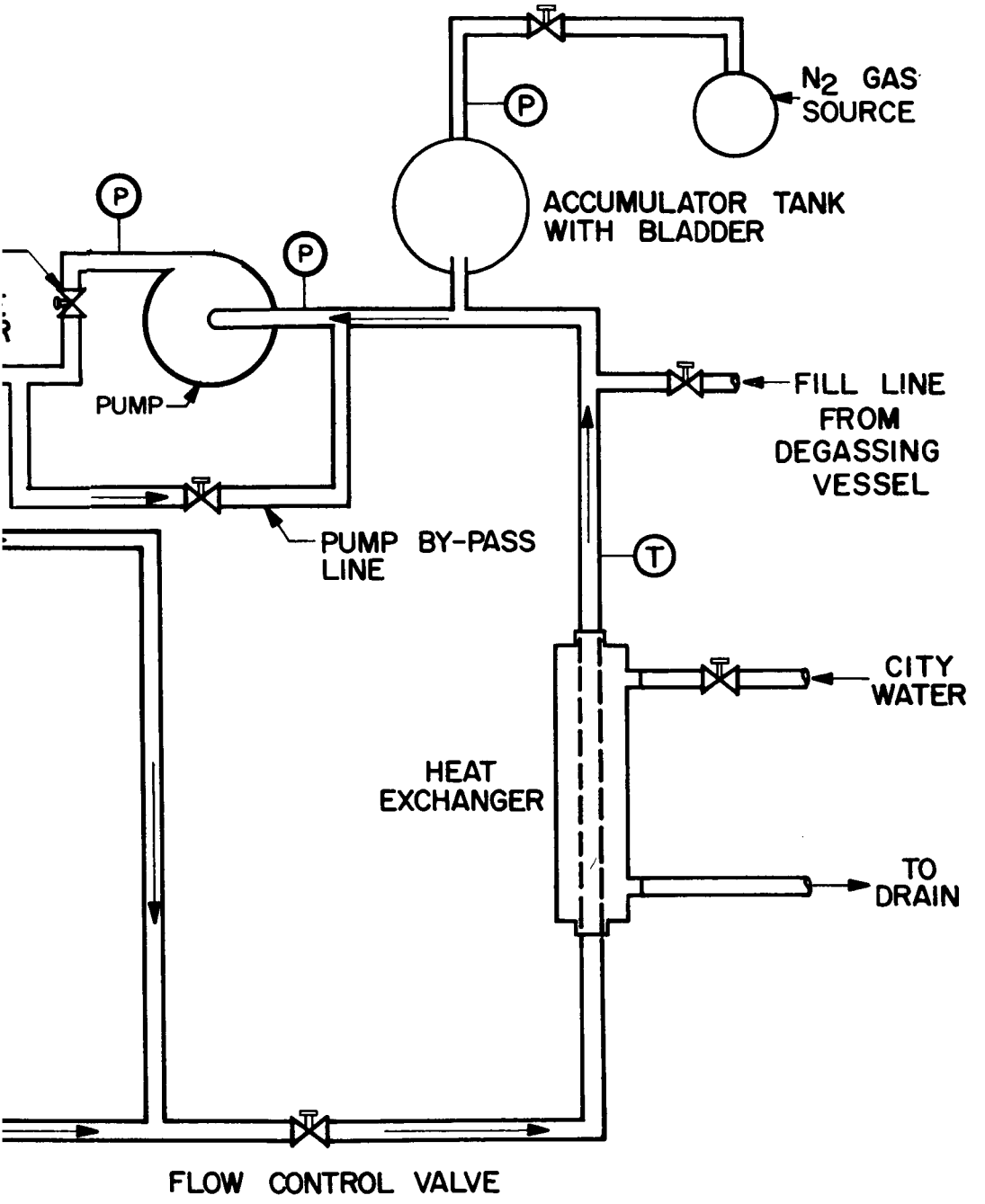
P
N_2 GAS SOURCE
ACCUMULATOR TANK WITH BLADDER
P
P
PUMP
FILL LINE FROM DEGASSING VESSEL
PUMP BY-PASS LINE
T
CITY WATER
HEAT EXCHANGER
TO DRAIN
FLOW CONTROL VALVE

)LDER

3

rates, and manometers to measure pressure drops. Also included in the permeability apparatus is a means of ensuring that the working liquid is not saturated with gas. Gas-saturated liquids may allow bubbles to form in the wick as test time progresses, causing K_1 to be a function of time. Desaturating the liquid of its gases is done by raising the liquid temperature with a resistance heater, causing the solubility of the liquid to decrease. The gas expelled from the liquid is collected and bled from a high point of the system. When the apparatus is returned to ambient temperature the system liquid is in an unsaturated state.

Figure 13 is a close-up photograph of the assembled permeability sample holder.

B. Initial Testing and Modifications to Permeability Apparatus

In checking out the apparatus no major changes were found to be necessary. A few minor modifications were found to be desirable, however, and these are discussed below.

As mentioned in the first quarterly report, the major foreseeable problem would be preventing K_1 from increasing with time while the flow rate was fixed. Previous experimenters found this occurrence and theorized that air, previously absorbed in the liquid, became trapped in the wick as bubbles. The trapped air blocked some flow passages and increased both the pressure drop and the apparent friction factor K_1. The permeability apparatus was designed to desaturate the working liquid by a heating and cooling procedure. With unsaturated liquid, the tendency to form bubbles should be reduced. In order to determine the capabilities of the apparatus to provide values of K_1 independent of time, initial tests were performed with water flowing through a stainless steel sintered fibrous metal wick. These tests indicated that during a run of 15-1/2 hours at a constant flow rate of 12.9 lb_m/hr, K_1 increased 25 per cent. Since other investigators[1] found that for water saturated with gas the flow through wicks was practically stopped during an endurance run, the degassing method appeared to be an effective solution of the problem. However, this method of degassing the liquid is limited in effectiveness because all the fluid in the apparatus cannot be desaturated. The fluid in the

[1] Ginwala, K., T. A. Blatt, and R.W. Bilger, Engineering Study of Vapor-Cycle Cooling Components for Space Vehicles, Tech. Doc. Rept. No. ASD-TDR-63-582, Sept. 1963, AF Flight Dynamics Laboratory, Air Force Systems Command, Wright-Patterson Air Force Base, Ohio, pp 120-148

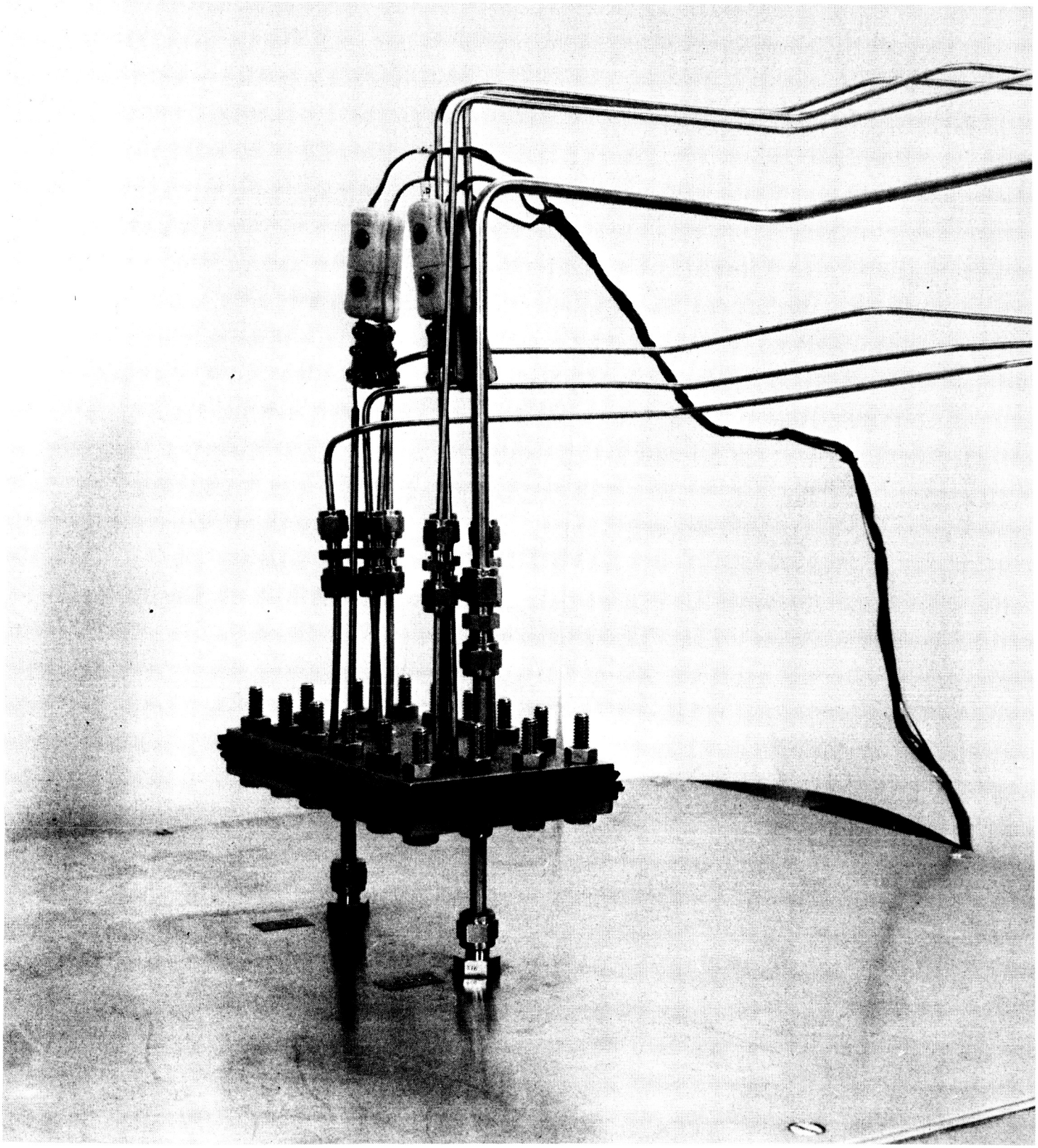

Figure 13 Sample Holder for Permeability Apparatus

pressure gage lines, U-tube lines, and the accumulator tank (see Figure 12) is not desaturated because it does not flow in the closed loop.

In an effort to make K_1 constant with time, an additional degassing apparatus was made. This apparatus is separate from the permeability apparatus, and its purpose is to supply completely degassed liquid for filling the permeability apparatus. This new apparatus is simply an air-tight vessel made from stainless steel and equipped to heat and boil about five gallons of liquid. Figure 14 shows the vessel in front of the permeability apparatus during filling. Although the filling procedure is explained in more detail below, the basic approach is as follows. The test liquid is put into the vessel and brought to a boil. The gas is expelled from the liquid due to the high temperature and bled from the vessel. This unsaturated liquid is then passed into the evacuated permeability system. The degree of saturation of the water in the permeability apparatus after filling with liquid from this vessel is estimated to be less than 20 per cent.

Liquid treated in this way yielded no gas when it was passed through the degassing section of the permeability system. Hence, a definite improvement in decreasing the degree of gas saturation was made by the addition of the degassing vessel. After filling the system with water from the new vessel, an endurance test run with the same sample and flow rate resulted in no increase of K_1 for a period of 25 hours. Thus the time-dependency of K_1 that has been found by other investigators would appear to be due to the presence of dissolved gas in the test liquid.

Another flowmeter was added to the permeability apparatus for checking readings of flow rate. A slant-tube manometer (Meriam, 30 inches long with a 6-inch vertical height) was also added to increase the accuracy at the smaller sample pressure drops.

C. Test Procedure for Permeability Apparatus

1. Filling the Permeability Apparatus

The following procedure describes the filling of the permeability apparatus, using the degassing vessel shown in Figure 14. Because the permeability accumulator tank holds about 2-1/2 gallons of liquid in reserve, this filling procedure will only be necessary after five or six samples are tested.

1) The permeability apparatus is drained of any fluid. This involves taking the apparatus apart at several locations and draining low points.

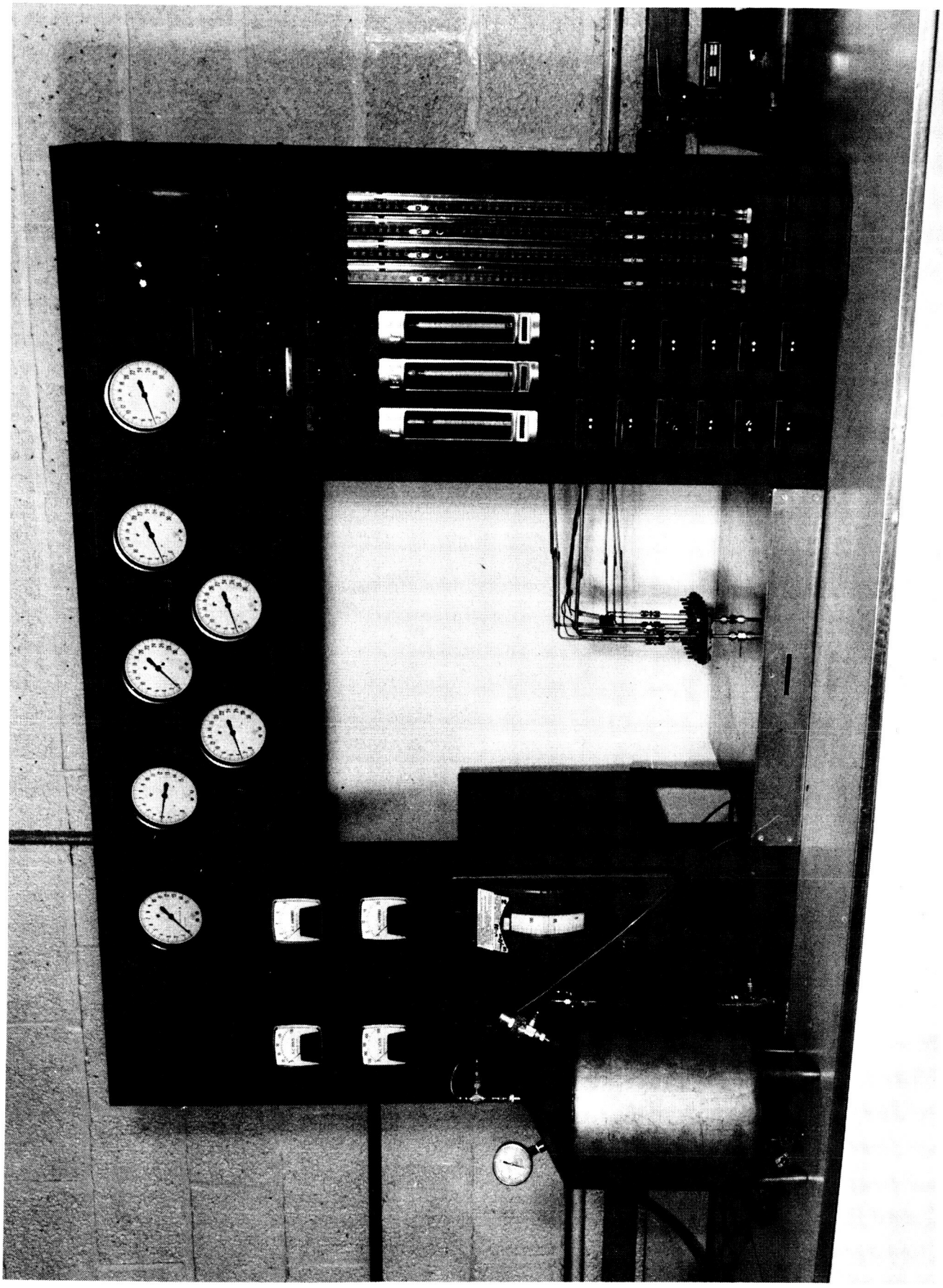

Figure 14 Wick Permeability Apparatus with Degassing Equipment in Place

2) Nitrogen gas is passed through the apparatus to evaporate any remaining fluid.

3) A vacuum pump is attached to the apparatus so that the entire system (without the wick holder) and the tubing connecting the apparatus to a liquid outlet valve on the degassing vessel are evacuated to a pressure no greater than 1 mm of Hg before filling starts.

4) The degassing vessel is filled with the test liquid, and the liquid is then brought to its saturation temperature. In practice, when the vessel heater is first plugged in, local boiling around the heater starts. However, several hours may be required to bring the entire vessel of water to its saturation temperature. During this process of heating, the valve at the top of the vessel is open for expelling both gas, which is expelled by the water, and water, which drains out because of its expansion. Eventually only vapor exits from the top valve on the vessel and a pressure can be built up in the vessel by closing the valve. A pressure between 2 and 5 psig is maintained by turning the heater on and off as a control.

5) With a pressure less than 1 mm of Hg in the permeability apparatus and a pressure of about 5 psig in the vessel, the liquid outlet valve on the vessel is opened. During the process of filling, the evacuation is continued at the highest point of the apparatus. When water in liquid form appears at the high point the vacuum pump is disconnected from the apparatus. A half hour or more may be required after initially opening the liquid valve to fill the apparatus. After the pressure of the apparatus becomes the same as the pressure in the vessel, the apparatus is valved off from the vessel. To fill the system with liquid usually requires two-thirds of the contents of the vessel.

2. Wick Permeability Testing Procedure

The wick permeability testing procedure is as follows:

1) The permeability apparatus (except for the sample holder) is filled with unsaturated liquid as described above.

2) Measurements of the wick dimensions necessary for evaluating K_1 are made.

3) The wick is cleaned using the same procedure as for the wicking rise samples.

4) The wick and sample holder shown in Figure 11 are assembled as shown in Figure 13.

5) The sample holder is filled with degassed liquid from the rest of the permeability apparatus by evacuating the holder to at least 1 mm of Hg and then opening the inlet and outlet sample valves (Figure 12). The evacuation is discontinued when the holder is full of liquid.

6) The U-tubes are bled, using the positive pressure in the permeability apparatus.

7) A testing program on the sample wick is conducted including runs with flows from 1 to 10 lbs/hr, runs at various wick fluid temperatures, and a time-duration run. The test data includes flow rates, temperatures, and pressure drops of the fluid flowing through the wick.

D. Test Results

The results now being obtained with the permeability apparatus are shown in Figures 15 and 16.

Figure 15 is a plot of wick friction factor versus flow rate for a sintered stainless steel fiber sample. For flow rates up to about 10 lb_m/hr, K_1 remained essentially constant, and for higher flows K_1 increased slightly with flow rate. This indicates that flow rates less than 10 lb_m/hr are within the Darcy flow regime where friction causes the only pressure drop. Flow rates above 10 lb_m/hr are outside the Darcy regime where inertia effects start to enter as a pressure drop component, causing K_1 to increase.

Figure 16 is a plot of wick friction factor versus time for the same sintered stainless steel fiber sample. This plot shows that K_1 does not vary with time since the small variation in K_1 of ±2 per cent is within the expected experimental accuracy.

E. Accuracy of Results

The frictional forces of flow through a wick are characterized by a friction factor K_1 given in Equation (2). Based on statistical analysis, a valid approximation to the uncertainty in K_1 is

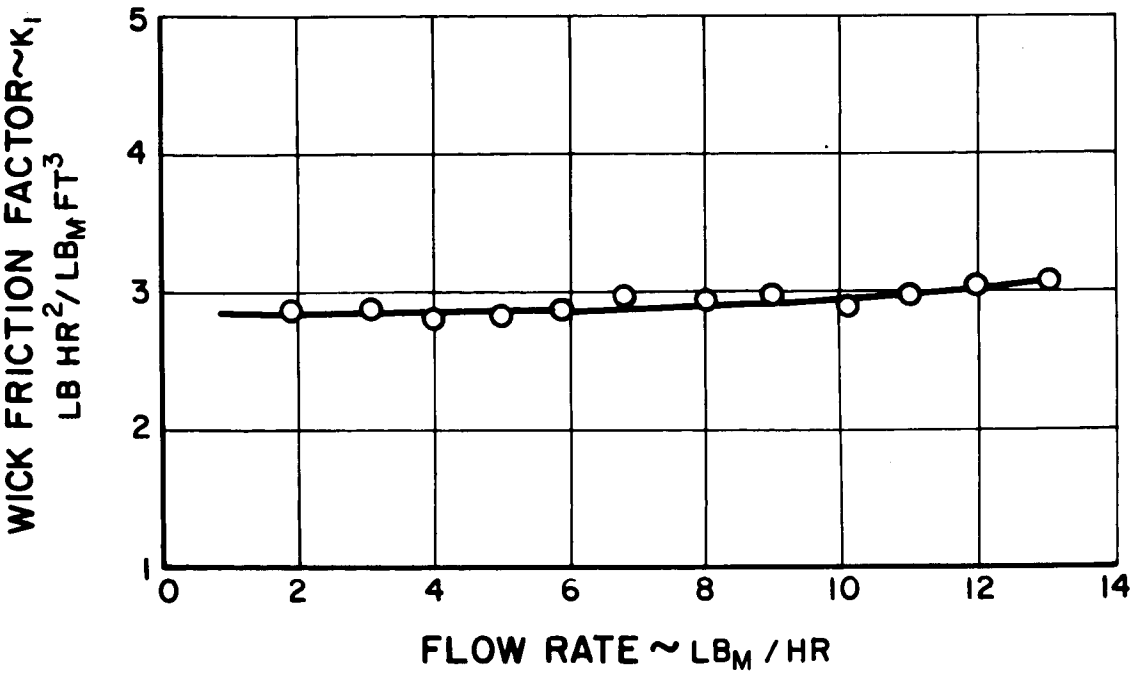

Figure 15 Wick Friction Factor vs Flow Rate for Sintered Stainless Steel Fiber Sample

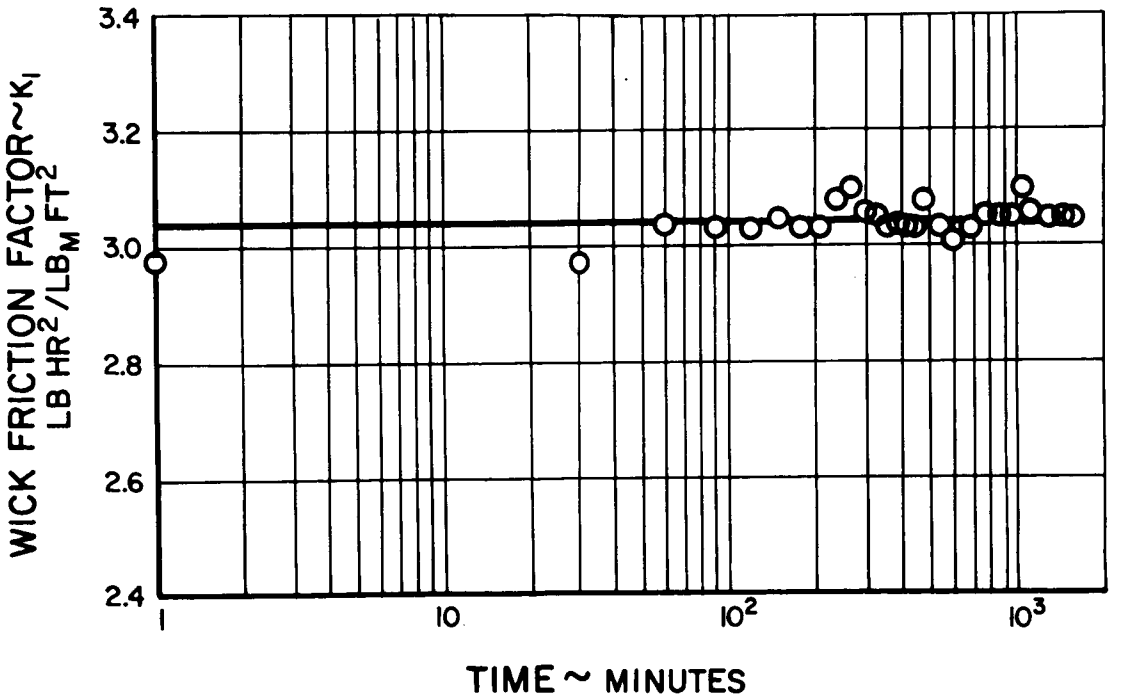

Figure 16 Wick Friction Factor vs Time for Sintered Stainless Steel Fiber Sample

$$\text{percentage uncertainty in } K_1 = 100\frac{dK_1}{K_1} = \left[\left(100\frac{dA_c}{A_c}\right)^2 + \left(100\frac{d\Delta x}{\Delta x}\right)^2 + \left(100\frac{d\rho_L}{\rho_L}\right)^2 + \left(100\frac{d\mu_L}{\mu_L}\right)^2 + \left(100\frac{d\Delta P}{\Delta P}\right)^2 + \left(100\frac{dw_L}{w_L}\right)^2\right]^{1/2} \quad (3)$$

In Equation (3), the quantity dK_1 is used to indicate that the true value of K_1 is in the range $K_1 \pm dK_1$ (with analogous meanings for dA_c, $d\Delta x$, $d\mu_L$, etc.). The values of $d\rho_L/\rho_L$ and $d\mu_L/\mu_L$ are made small by running the apparatus at constant temperature. The uncertainties of the sample dimensions results in

percentage uncertainty in cross-sectional flow area

$$= 100\frac{dA_c}{A_c} = \left[\left(100\frac{d\,\text{width}}{\text{width}}\right)^2 + \left(100\frac{d\,\text{depth}}{\text{depth}}\right)^2\right]^{1/2} \approx 2\% \quad (4)$$

and

$$\text{percentage uncertainty in flow length} = 100\frac{d\Delta x}{\Delta x} \approx 1\% \quad (5)$$

The above estimates include instrument accuracy and nonuniformity of the wick due to fabrication. The values of $d\Delta P/\Delta P$ and dw_L/w_L are functions of the amount of flow. Assuming that it is possible to maintain steady conditions in the permeability rig, the accuracy of ΔP and w_L will be the same as the accuracy of their respective measuring devices. The percentage uncertainty of the low-range flowmeter varies from ±7 per cent at a flow of 0.4 lb_m/hr to ±1.8 per cent at 1.45 lb_m/hr. For the high-range flowmeters, the accuracy varies from ±5 per cent at 1.45 lb_m/hr to ±1 per cent at 14 lb_m/hr. The uncertainty in the slant-tube manometer used in the low pressure drop measurements varies from ±1 per cent at ΔP = 0.0340 psi to ±0.5 per cent at ΔP = 0.412 psi. For higher pressure drops, where a U-tube manometer is used, the accuracy ranges from ±1 per cent at ΔP = 0.412 psi to ±0.5 per cent at ΔP = 1.370 psi. Hence the maximum percentage uncertainties in flow and pressure drop are:

$$100\frac{dw_L}{w_L} \approx 7 \text{ per cent} \quad (6)$$

$$100\frac{d\Delta P}{\Delta P} \approx 1 \text{ per cent} \quad (7)$$

Using Equation (3) and the values from Equations (4) to (7), the percentage uncertainty of the friction factor K_1 is:

$$100\frac{dK_1}{K} \approx 7.4 \text{ per cent} \quad (8)$$

VI. WICK BOILING STUDIES

The purpose of the boiling tests is to:

1) measure the maximum heat fluxes that a saturated wick-covered surface can sustain before film boiling occurs, and

2) find out how these limiting heat fluxes vary with the wicking material, the boiling fluid (water or Freon 113), wick orientation with respect to gravity, and degree of wick saturation.

These results will be interpreted to determine limitations in fin operation imposed by the boiling region of the fin. Also, from the recorded data, boiling heat transfer coefficients will be calculated. This section contains a description of the boiling test rig, the test procedure and data obtained in the process of rig checkout.

A. Description of Boiling Apparatus

1. Overall Design

A sketch of the boiling rig primary tank is shown in Figure 17. Photographs of the overall setup and a closeup of the primary tank are shown in Figures 18 and 19. The rig consists of a sample-heater assembly, mounted on copper busbars, firmly pressed against insulating blocks by means of busbar adjusting screws. The wick boiling sample consists of a piece of porous nickel or stainless steel 2.875 by 0.625 by 0.10 inch thick, bonded to a backup plate of the same material. The boiling samples are cut from the wicking samples shown in Figure 1. The sample and the heater are bonded together to provide good thermal contact without electrical contact. Current flows only through the heater. The insulating blocks, two of which have a Nichrome guard heater sandwiched between, rest on a Textolite platform, which is mounted in the stainless steel primary tank. The Plexiglas cover and Neoprene gasket are used to prevent spillage during the tests in which the primary tank is tilted. Due to the small size of the sample, there is in general little resistance to fluid flow in the wick. Hence, the limiting factor in the determination of the maximum possible heat flux through the wick should be the onset of film boiling, rather than the wicking ability of the sample.

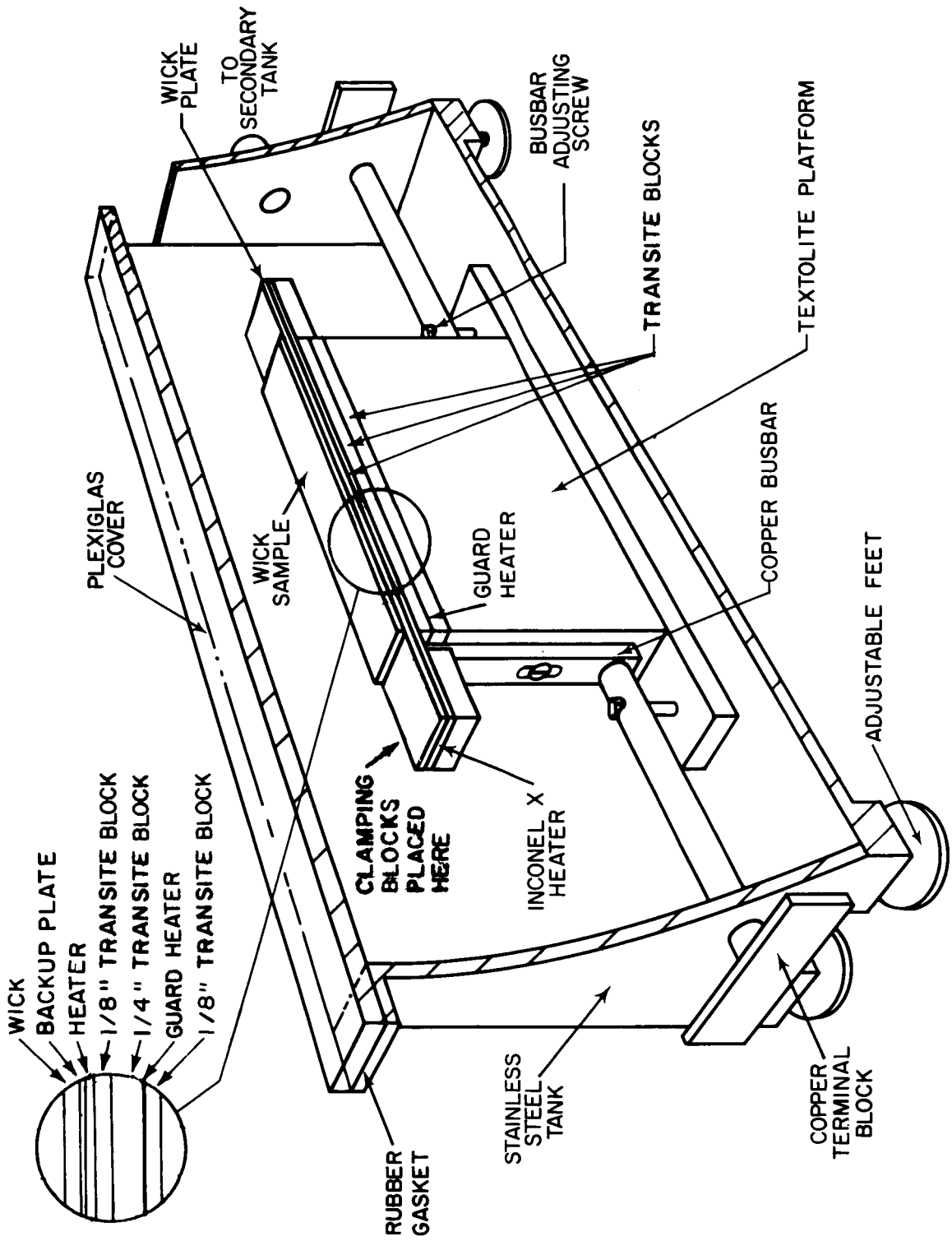

Figure 17 Cutaway View of Boiling Test Apparatus

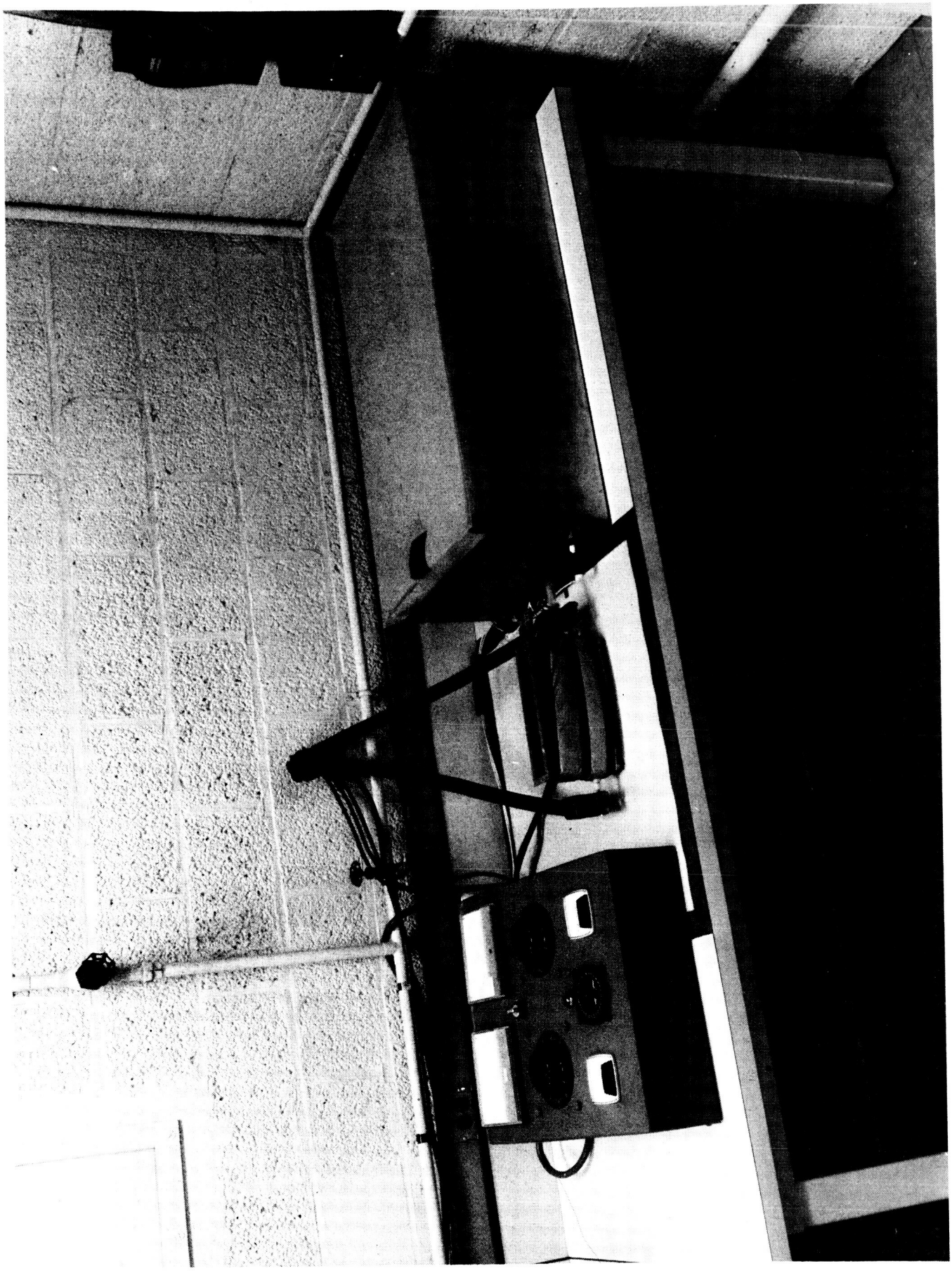

Figure 18 Wick Boiling Experimental Test Setup Showing Control Panel, Primary Tank, and Secondary Tank

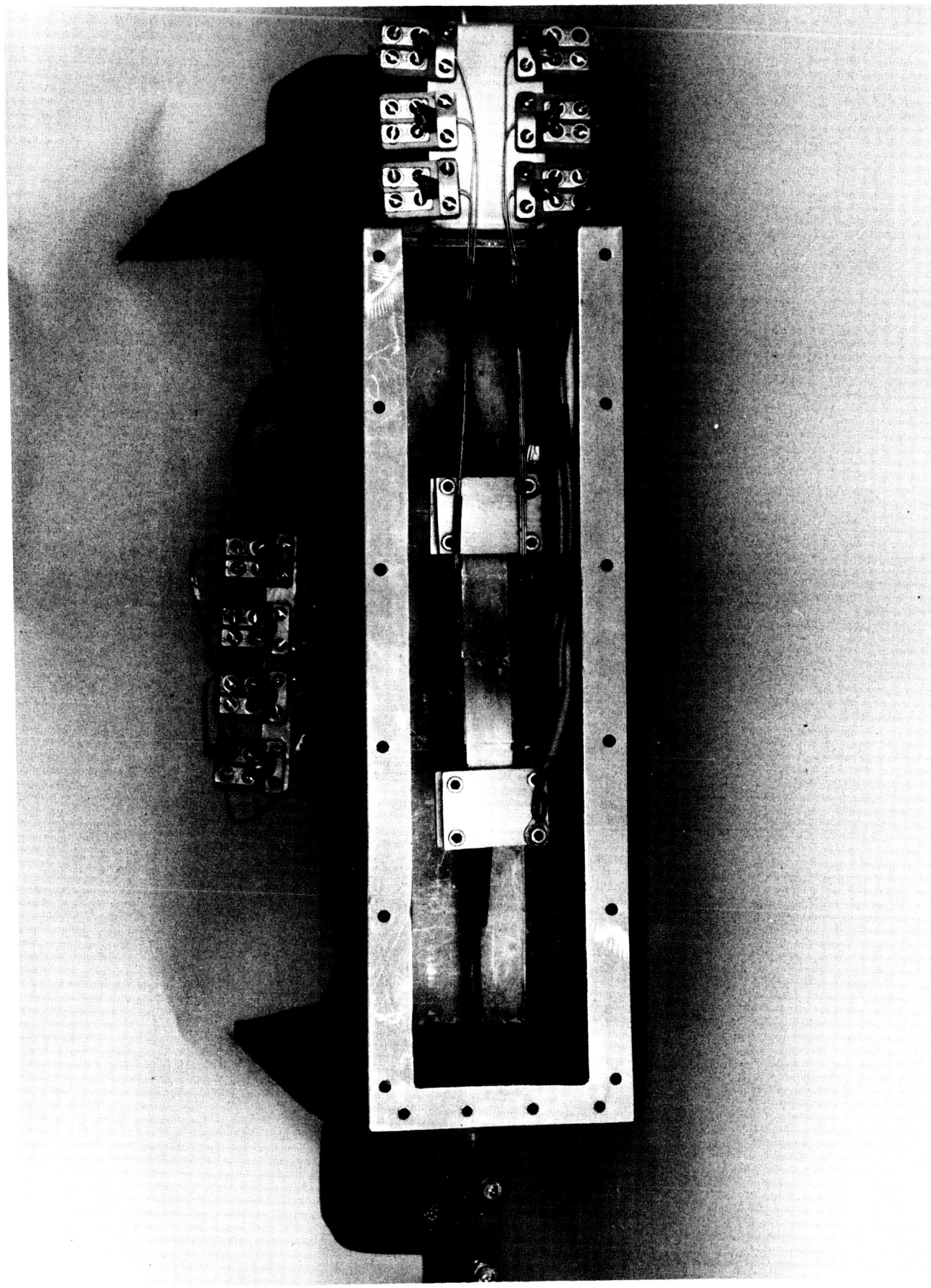

Figure 19 Top View of Primary Tank with Flat-Plate Sample Installed

In order to reduce the stresses that the bonding material between the heater and the sample must withstand due to differential thermal expansion between these components, heaters of Inconel X750 will be used with nickel samples and a stainless steel heater will be used when testing the stainless steel samples.

As a result of preliminary testing (described in Section VI. C. below), the following changes in the boiling rig primary tank assembly have been made since the last report period.

The magnesium oxide insulating blocks have been replaced by Transite blocks because the magnesium blocks cracked in several tests. Transite, which is a good thermal insulator and able to withstand relatively high temperatures, is less brittle than magnesium oxide.

It was found unnecessary to braze the heater to the copper busbars. Instead, the heater and sample are clamped to the busbars by the brass-Transite holding blocks (Figure 19). Gold foil between the busbar and heater insures good electrical contact.

The heater-sample assembly has been altered. The assembly, shown in detail in Figure 17, now consists of the heater, coated with 2 mils of aluminum oxide, bonded to the sample with epoxy resin. A 1/8-inch Transite block is then held to the bottom surface of the heater by a layer of epoxy which bonds the edges of the heater, sample backup plate, and Transite. The photograph of the instrumented sample in Figure 20 shows this edge of epoxy. The advantages of this design are the following:

1) The aluminum oxide coating provides the electrical resistance necessary to prevent current leakage across the sample, while the thermal conductivity remains quite high for an electrical insulator (10 Btu/hr ft^2 °F). Hence, the temperature drop across the aluminum oxide at the maximum design heat flux of 500,000 Btu/hr ft^2 °F is only 10°F compared to 125°F for the previous mica-insulated design.

2) The epoxy bond between the heater and sample insures good thermal contact.

3) The epoxy edge prevents boiling heat transfer losses from the edges of the sample backup plate and heater (edge boiling could also inhibit the flow of fluid to the wick surface).

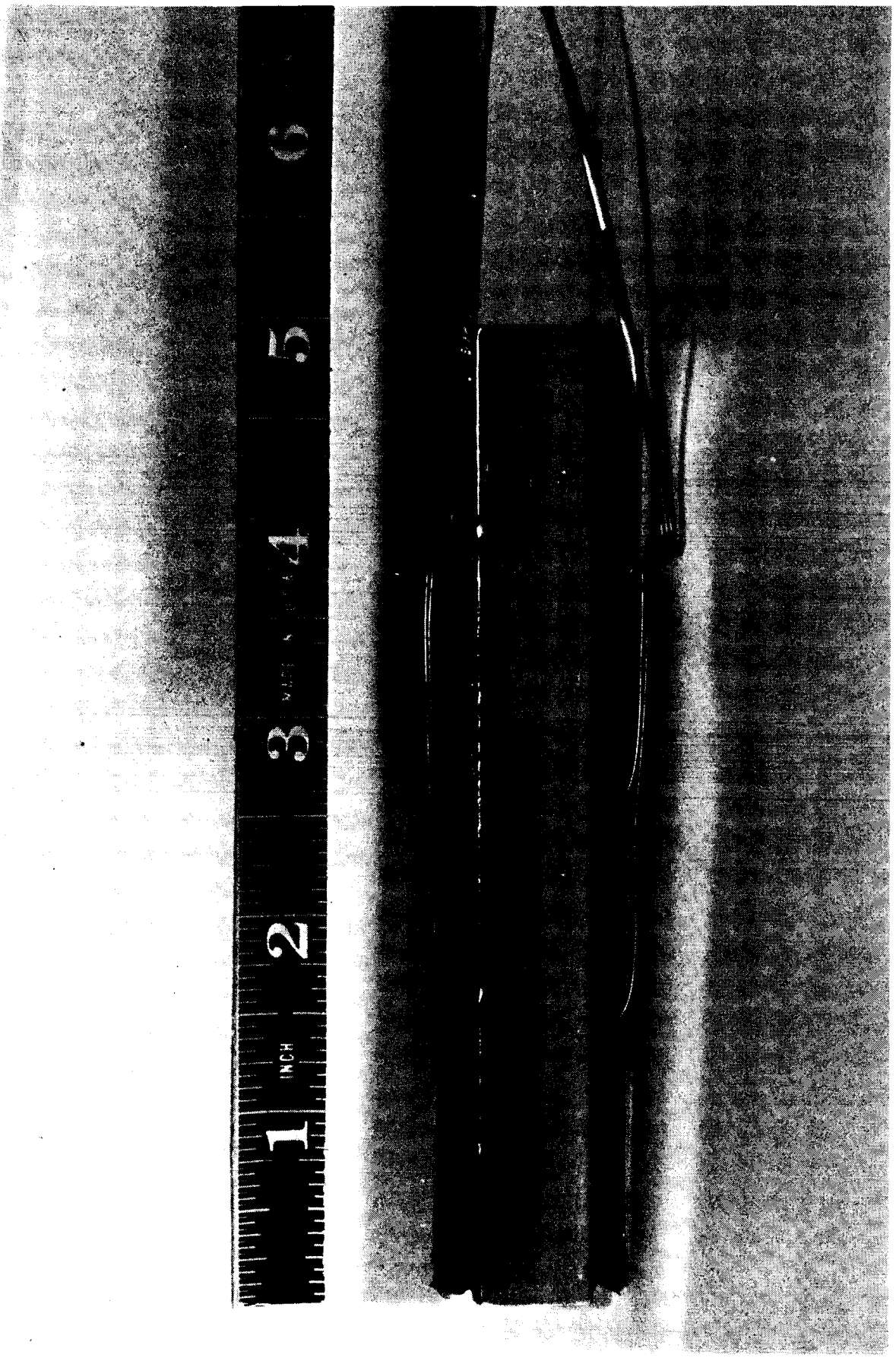

Figure 20 Instrumented Flat-Plate Boiling Test Sample

4) The Transite prevents boiling from the bottom of the heater. The Transite is held in place by the epoxy on the edges of the assembly, rather than the underside of the heater, because the heater underside is at the highest temperature of any surface in the boiling apparatus. Hence, it is possible that the epoxy would decompose at this surface.

5) The present heater sample design is more durable during assembly than the previous mica-insulation design. The latter design consisted of a 0.0003-inch thick strip of mica insulation between the sample and heater, with the heater and sample bonded to the mica. Mica can be torn quite easily by burrs on the sample and by mishandling.

A photograph of the overall setup, including primary tank, control panel, and secondary tank is shown in Figure 18. The large surface area of the secondary tank limits the change in liquid height with time, as boiling occurs, to a negligible value. A heater in the secondary tank maintains the water entering the primary tank at near saturated conditions. A modification being made to the rig will provide a heater between the two tanks to replace the secondary tank heater. This design will eliminate the long heat-up time required for the secondary tank water. It will also be a more efficient method of heating the fluid entering the primary tank, since the heater will only heat that quantity of liquid required to replace the fluid that boils away.

2. Power Supplies

Power for the boiling rig heater is supplied by a 12 KVA rectifier with a three-phase 480-volt input and a controllable output of up to 750 amperes at 12 volts, or 1500 amperes at 6 volts.

The guard heater power is controlled by a 115-volt input powerstat.

The secondary tank heater is a 5 KW 230-volt resistance type, controlled by a powerstat.

3. Instrumentation

The data obtained from the boiling tests will be used to plot ΔT_{SAT}, the temperature difference between the saturated vapor and the liquid-wick-solid interface, as a function of the resultant heat flux through the wicking sample. In order to accomplish this, six chromel-alumel thermocouples are located in the underside of the sample backup plate to measure wall temperatures, two thermocouples are used to measure the temperature of the saturated vapor, and two are immersed in the boiling water. Also, two sets of thermocouples are located at different planes in the Transite block on top of the guard heater. For each test point, then, the guard heater is adjusted until the two sets of thermocouples read the same value, thus showing zero heat losses from the underside of the heater. The heat flux Q is computed from the measured voltage drop and current across the sample, and the known area of the sample.

Figure 20 shows six thermocouples installed in a flat-plate test sample. The thermocouple sheaths (0.010 inch in outside diameter) are welded in 0.015-inch grooves. The actual thermocouple wire (0.001 inch in diameter) is then welded to the bottom of the groove. Hence, the temperature being measured is 0.015 inch from the surface of the sample. For the wick samples the same construction will be used, except that the grooves will be machined in the underside of the wick backup plate. Since the backup plate is 0.025 inch thick, the temperature measured will be 0.010 inch from the liquid-wick-solid surface. The liquid-wick-solid interface temperature can be calculated by

$$T_{lws} = T_m - (Q/A)(\Delta x/k) \qquad (9)$$

where

T_m = measured temperature in backup plate
Q = heat input to sample
A = heater area normal to heat flow
Δx = backup plate thickness from measured temperatures to the liquid-wick-solid interface (about 0.010 inch)
k = thermal conductivity of the backup plate

B. Test Procedure

1. Tank Filling

The boiling tests begin by filling the secondary tank with the test fluid to the approximate level desired in the primary tank. The hose clamp in the line connecting the two tanks is then opened, allowing the fluid to

flow from the secondary tank, through the heater, to the primary tank. The heater will be adjusted so that the primary tank is filled with the fluid at a temperature just below saturation. Fine adjustments on the liquid level in the primary tank will be made by altering the adjustable feet on the primary tank, or by adjusting the level of liquid in the secondary tank.

2. Nucleate-Boiling Region

Power to the primary heater is controlled by means of a motor-controlled powerstat to the 12 KVA rectifier unit. At low power levels (i.e., not near film boiling), the data points will be taken at increasing intervals of 25,000 Btu/hr ft^2 in heat flux. At each point the guard heater will be adjusted, by means of a 110-volt powerstat, until the temperatures of the top two Transite block thermocouples read the same as the bottom two (indicating zero heat loss from the bottom of the heater through the Textolite block). The temperatures will be recorded after stabilizing to a point where there is no change over a three-minute period. The heater voltage, and current, and the guard heater current, will also be recorded. Adjustments in the liquid level can be made between data points, if necessary (the decrease in water level is 0.018 inch for a 10-minute run at a heat flux of 500,000 Btu/hr ft^2).

Repeatability of data points will be spot-checked throughout the tests. Possible hysteresis effects will be checked by approaching some data points from both a higher heat flux level and a lower level.

3. Film-Boiling Region

The approach of the film-boiling regime can usually be detected by visual observation of the bubbles in the nucleate-boiling regime (a relatively large number of nucleation sites with relatively large bubbles). From this point on, the power level interval at which data is recorded will be decreased to 5000 Btu/hr ft^2. At the onset of film boiling, as evidenced by a sharp rise in sample temperatures, the test will be terminated by shutting off the electrical power.

C. Preliminary Tests

Sixteen preliminary tests have been run with the instrumented flat-plate sample (Figure 20). The results of these tests were as follows.

In order to attain heat fluxes as high as 500,000 Btu/hr ft^2, it is necessary to have a low thermal contact resistance between the heater and

sample. It is also required, however, to have these two components electrically insulated from each other. From visual inspection, it was apparent that these two requirements could not be satisfied by simply clamping the heater and sample in the rig with a sheet of mica insulation between them. The reason for this condition is that gaps appear between the two surfaces, between the two clamped ends. In fact, gaps are evident even when the two surfaces are precision-ground to within ±0.0005 inch. Hence, it is necessary to bond the sample to the heater. In the preliminary tests various bonds and techniques were attempted. Some of the more significant results were the following:

1) A silicone rubber cement was spread on the upper heater and lower sample surfaces. A sheet of mica (0.0003 inch thick) was then placed between them, and the whole assembly was clamped together as the cement dried. This combination performed well, and a measured heat flux of 378,000 Btu/hr ft^2 was attained. However, after sustained testing, sections of the cement started to decompose.

2) A thicker coating of another rubber cement was tried without the mica insulation. The sample proved to be electrically insulated from the heater, but the thermal resistance was too high.

3) An epoxy-mica-epoxy combination was tested (Figure 20). This design performed well.

4) One side of the heater was plasma-sprayed with aluminum oxide and bonded to the sample with an epoxy. This combination performed well, and, to date, is the best method found. The advantages of this design are outlined in Section VI.A. above.

The preliminary tests were run to check out the rig, including critical points such as the electrical contact surfaces between the busbars and heater, the guard heater, and the lead wires. The results of these tests led to the design modifications outlined in Section VI.B. above. The guard heater is not yet functioning properly and it appears that a higher powered guard heater will have to be installed.

The preliminary tests were also run to obtain data on a flat-plate sample for comparison with published results. The flat-plate sample had six thermocouples installed on its upper surface, as shown in Figure 20. A plot of the sample temperature as a function of heat flux is shown in Figure 21, for two of the tests made. The temperature shown is taken from one of the six thermocouples. Because all of the thermocouples were not located at the same depth, readings from the other five may

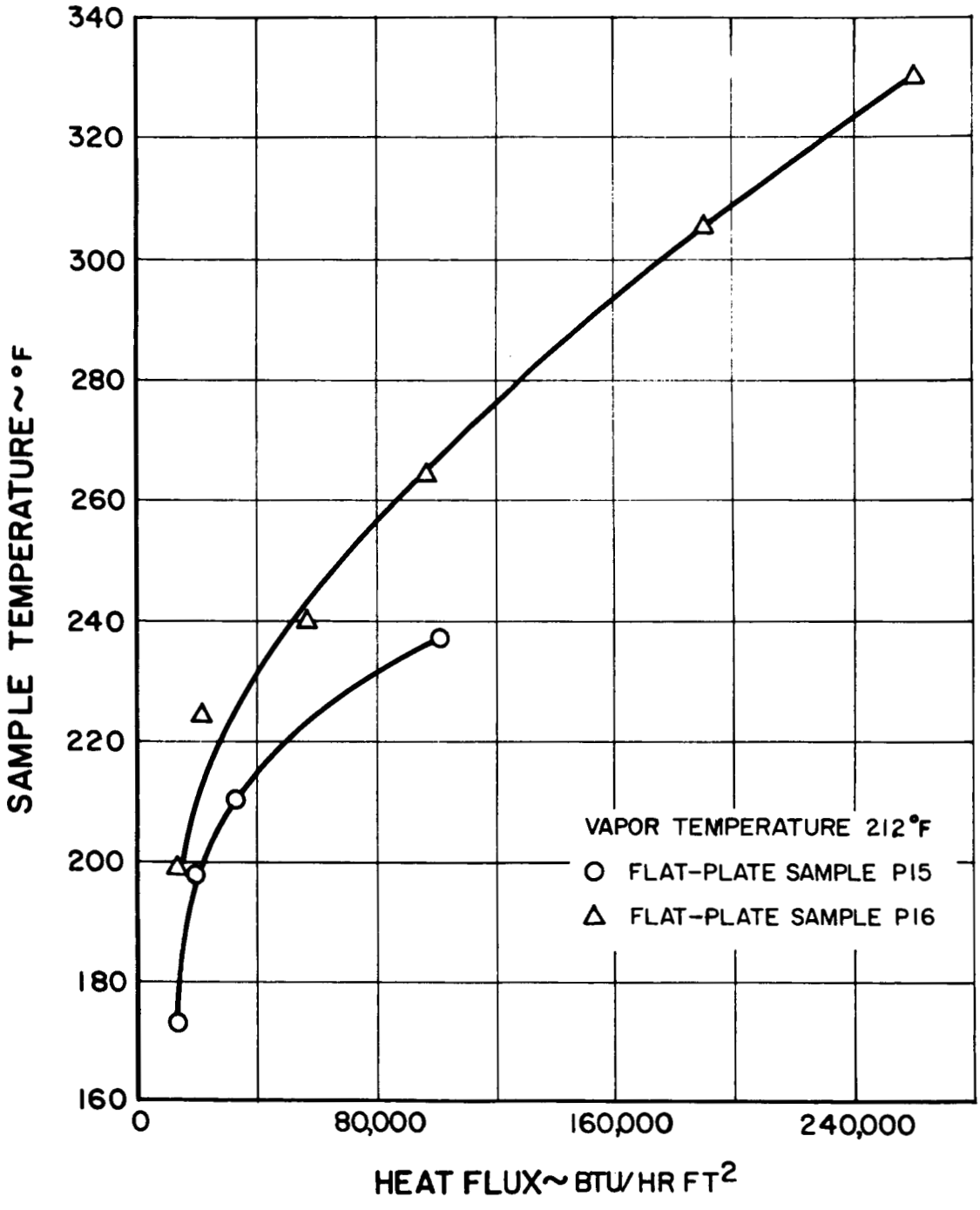

Figure 21 Sample Temperature vs Heat Flux for Boiling Heat Transfer from Horizontal Flat-Plate Samples (Preliminary Data)

not have been exactly the same as that shown in Figure 21, but all gave the same curve shape.

The two tests represented in Figure 21 employed an epoxy-mica-epoxy sample heater bond and were run on successive days. Between the two tests the sample was smoothed down with emery and cleaned with acetone.

The accuracy of the results is questionable in both tests since the guard heater was not functioning correctly, the primary tank insulation was not yet in place, and the secondary tank heater was not yet operating. However, several general observations can be made from the data.

1) The general shape of both curves agrees with the published data[3] for boiling off of a flat plate. In Figure 21 the slope of the curves is steep at low heat fluxes, showing that the primary mode of heat transfer is natural convection, followed by a flattening of the curve as boiling sets in.

2) For the same heater temperature, a greater heat flux was evident in Test P15 than in Test P16 (in other words, the curve shifts upward from P15 to P16). This superior boiling heat transfer is due to the greater number of bubble nucleation sites on the rougher surface of P15 as compared to P16. This result also agrees with the published data[1].

3) At the last recorded point the boiling was quite vigorous. As the power to the heater was further increased to about 300,000 Btu/hr ft^2, the sample temperature increased rapidly to about 650°F. The test was then terminated. It appears that the onset of film boiling occurred at this point.

At the conclusion of the test it was observed that the sample buckled and hence separated from the heater. This was caused by the differential thermal expansion, at the high temperatures, between the nickel sample and stainless steel heater. These components will be fabricated from the same material in future tests.

At present, tooling for the electrochemical machining process described in Section III. E. above is being designed and built. This tooling is necessary to cut the porous samples for the boiling studies. Cutting the samples by other means would close the pores on the sides of each sample, thus prohibiting heat transfer tests in which the degree of wick saturation could be varied.

[1] Jacob, Max, Heat Transfer, Volume I, p 637, Wiley, 1959

VII. FUTURE WORK

A. Task 1 - Wicking Studies

Wicking rise tests on samples received from suppliers will be continued during the next quarter. Because these tests have been found to be so time-consuming, another wicking apparatus similar to the one described in Section IV will be built, so that 10 to 11 samples can be tested at one time.

To prevent any delay in further permeability testing, permeability samples will be cut from the ends of the wicking samples, if necessary, before wicking tests are run on samples. In all cutting operations the electrochemical machining technique discussed in Section III will be employed.

Permeability testing will continue. Initially the wick friction factor of all wicking samples will be measured with enough testing to ensure that the K_1 so determined is in the Darcy flow regime. On the samples that prove to have a high value of l_m/K_1, more detailed permeability testing will be done, over wider flow rate ranges and fluid conditions. Also, on the more promising samples, pore size distribution, equivalent pore diameter, and the mean pore radius will be determined.

B. Task 2 - Boiling Studies

Further flat-plate data will be taken, both to evaluate the boiling apparatus by matching published data, and to work out any further problems associated with the apparatus.

As soon as some preliminary data on the l_m/K_1 for the wicking samples is obtained, samples will be cut by the ECM method. Following their instrumentation with thermocouples, the samples will be tested in the wick boiling apparatus.

C. Tasks 3 and 4 - Vapor-Chamber Fin Studies

Two experimental vapor-chamber fin model designs are being investigated. One employs liquid convective cooling as a means of heat rejection, while the other uses radiation. Both models are flat-plate wick designs and both are heated electrically. Further fin design will be conducted during the next quarter using the data obtained in both the wicking and boiling studies.